Aalto University
School of Chemical
Engineering

Mhd Adel Assad

Vacuum Evaporative Deposition of Photochromic Spirophenanthroxazine Thin Films and their Solvato-bleaching Feature

School of Chemical Engineering.
Major/Minor: Functional Materials/ Fibre and Polymer Engineering

Master's thesis for the degree of Master of Science
In Technology submitted for inspection.

Espoo 29.07.2019

Supervisor: Prof. Dr.-Ing. habil. Mady Elbahri
Advisors: M.Sc Ahmed Soliman & M.Sc Mehmet Yetik

Aalto University
School of Chemical
Engineering

Aalto University, P.O. BOX 11000, 00076 AALTO
www.aalto.fi

Abstract of master's thesis

Author Mhd Adel Assad

Title of thesis Vacuum Evaporative Deposition of Photochromic Spirophenanthroxazine Thin Films and their Solvato-bleaching Feature

Degree programme Master's Programme in Chemical, Biochemical and Materials Engineering

Major/minor Functional Materials/ Fibre and Polymer Engineering **Code** CHEM3025/CHEM3024

Thesis supervisor Prof. Dr.-Ing. habil. Mady Elbahri

Thesis advisor(s) M.Sc Ahmed Soliman & M.Sc Mehmet Yetik

Date 29.07.2019 **Number of pages** 59+5 **Language** English

Abstract

Stimuli-responsive materials are the major contributors to functional materials that play a significant role in many fields such as sensors and actuators. Among these materials photochromic molecules has attracted both the scientific and industrial communities, due to their unique features. When exposed to UV radiation photochromic materials would either exhibit isomerization (e.g. trans-cis / cis-trans), or result in a ring opening /closure, which would result not only in a change in their absorption spectrum, but also in their chemical and physical properties such as refractive indices, dielectric constants, oxidation-reduction potentials and geometrical structures. The embedment of photochromic molecules particularly Spirooxazine within a polymer matrix has been studied significantly in literature, yet due to its synthesis limitations standalone systems including the transformation from particle/cluster, to percolation and finally to a continuous film were never reported to the best of our knowledge.

Thus, herein we introduced the deposition of standalone Spirooxazine thin films via evaporative deposition with emphasis on the percolated and continuous film samples. The particle/cluster deposition of SPO is being extensively studied elsewhere by our group under the framework of ASCI project. The deposited films were studied for their chemical integrity, thickness, crystallinity, density, and photochromic ability. In addition, the deposited films decay kinetics were studied under both constant temperature and the influence of multiple volatile organic compounds (VOCs) such as Acetone, Acetonitrile and Isopropanol. Where a new unreported term, Solvato-bleaching, was assigned to describe the color fading kinetics upon VOCs exposure.

It was determined that the solvato-bleaching rate of the deposited film is dependent on the polarity of the solvent, so that with decreasing polarity the rate increases. However, some exceptions may take place when the surface morphology changes, thus we assume that the interaction is a surface limited interaction.

Keywords Physical Vapor Deposition, Photochromic molecules, Solvato-bleaching

Acknowledgment

{يَرْفَعِ اللَّهُ الَّذِينَ آمَنُوا مِنكُمْ وَالَّذِينَ أُوتُوا الْعِلْمَ دَرَجَاتٍ}

[المجادلة: 11]

{God elevates those among you, who believe,
and those given knowledge, many steps}
58:11

First and foremost, I would like to thank my supervisor, Prof. Mady Elbahri, for continuously giving me all the time, support, and motivation I needed. I could not have imagined having a better supervisor and a mentor, who opened my eyes to the beauty of the Nano world.

Besides my supervisor, a huge thank you for both my advisors M.Sc Ahmed Soliman and M.Sc Mehmet Yetik for their guidance, advice, and for answering tons of my never-ending lame questions.

I also would like to express my sincere gratitude to my family: my parents Mustafa Assad and Haifa Alchabi; and my siblings: Dana, Lujain, Malak and Aya for their unlimited love, support, encouragement and sacrifice.

In addition, I am very grateful for all the support and encouragement that I have received throughout my studies from all my friends and family, including my two flat mates Omar Numan and Abdulghani Aljayyousi.

Finally yet importantly, a heartfelt thank you goes to my first supervisor and close friend Dr. Abdul Hai Alami, for whom I wouldn't be here without his advice and guidance.

Adel Assad
July 2019, Espoo, Finland

Contents

1 Introduction

By convention, nanomaterials are materials, which has at least one dimension in the nanoscale [1]. These materials are usually subdivided into quantum dots that has all three dimensions in the nanoscale, nanowires which has both their x and y radii in the nanoscale, and finally thin films where only their thicknesses are in the nanoscale. Moreover, the better understanding of these nanomaterials has resulted in numerous developments in the fields of energy [2], biomedical [3], catalysis [4] and sensors [5].

Thin films play an important role in state-of-the-art technology. These films are considered the base of the information revolution [6]. Nonetheless, their better material utilization and interesting functionalities, has promoted thin films as a competitive candidate to be used in the development of new technologies and futuristic applications [7].

Additionally, one class of stimuli-sensitive thin films are photo-responsive thin films, that usually consists of photochromic molecules imbedded in a matrix usually a polymer [8]. Whereas with the exposure of UV radiation, photochromic molecules either exhibit isomerization (e.g. trans-cis / cis-trans), or result in a ring opening /closure [9].

The aim of this work is to evaporate and deposit organic photochromic Spirooxazine molecules through the means of evaporative deposition. Where these films will be studied for their chemical integrity, crystallinity and photochromic ability to be switched from the closed colorless form to the open colored form. In addition, the aim of this work is to study the decay kinetics, from open to closed form, upon the exposure of multiple volatile organic compounds such as acetone, acetonitrile, and isopropanol.

This thesis is subdivided into four main chapters, Chapter 2: Theoretical background, Chapter 3: Materials and Methods, Chapter4: Results and Discussion and lastly Chapter 5: Conclusion. In chapter 2, the current vacuum deposition methods are introduced, followed by a discussion on the evaporation thermodynamics and principles. Later on, the chapter introduces the parameters affecting the evaporation deposition of materials and the nucleation and growth of thin films. Thin films properties, materials and applications were also introduced before a discussion on organic photochromic materials in general and Spirooxazine in particular. Chapter 3 involves a detailed explanation of the materials and methods used in this work, whether to deposit or analyze thin films. Chapter 4 then presents the findings and the research

outcomes of the experimental parts. Lastly, Chapter 5, includes a summary of the highlighted outcomes and finding obtained.

2 Theoretical background

2.1 Thin film vacuum deposition methods

As technologies develop, the demand on thin film is exponentially growing since they are the main contributors to the information revolution [6]. Thus, many deposition techniques are utilized to deposit thin films. Each deposition method is distinct from the perspectives of operation, application, precursor materials and limitations.

2.1.1 Chemical Vapor Deposition

Chemical vapor deposition (CVD) is a deposition technique that consists of many types such as Hot Wall CVD, Plasma Enhanced CVD (PECVD) and Low Pressure CVD (LPCVD). In all of its forms CVD technique, employs thermal energy to activate a chemical reaction starting from the imported gaseous precursors and ending in a thin film on the substrate's surface [10].

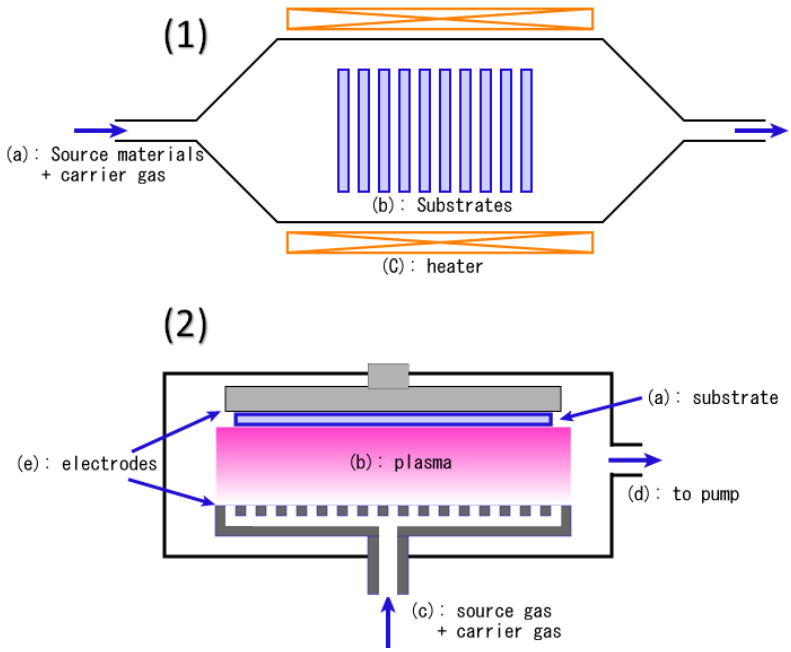

Figure 1.Chemical Vapor Deposition techniques schematics, 1) Hot Wall CVD, and 2) Plasma Enhanced CVD. Images obtained from the Public Domain.

CVD technique can not only be utilized to deposit thin films but also to deposit high purity bulk materials at deposition rates ranging between 0.1 to 10 nm/s. One of the most common material to be deposited via CVD is silicon, which follows the following reaction [11].

$$SiH_4\,(g) \rightarrow Si\,(s) + 2H_2 \qquad \sim 600°C \qquad (1)$$

When the volatile precursor(s) are being pumped into the CVD chamber, they travel by convection towards the pump; however, some of the precursor(s) diffuses into the boundary layer towards the substrate surface where the chemical reaction takes place. Subsequent to the chemical reaction, the byproducts are desorbed and transport back into the convection current to be pumped away, while the deposited materials are adsorbed to the surface.

2.1.2 Atomic Layer Deposition

Atomic layer deposition (ALD) is a deposition method that enables the growth of high quality ultrathin films, that possess a uniformal, conformal, and pinhole-free distribution [12]. ALD is considered a special type of CVD [13], yet unlike CVD, in which the deposition would continue as long as the precursors are added; ALD is surface limited reaction, as means to that the chemical reaction stops after the entire surface reacts no matter how much precursor was introduced.

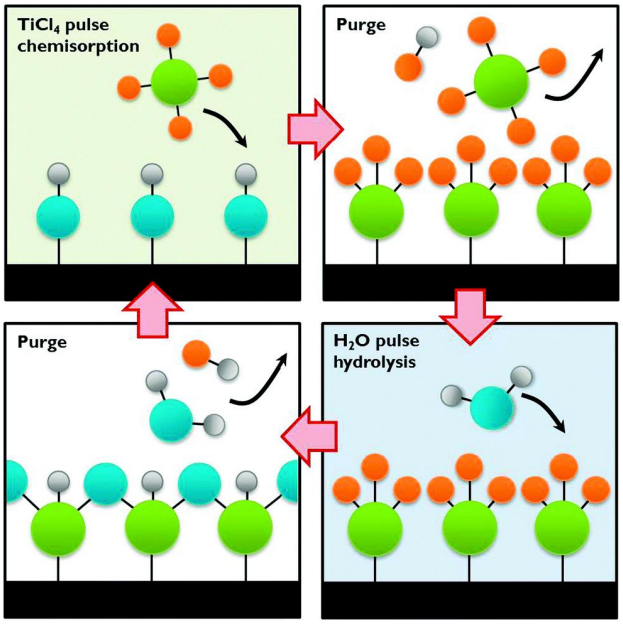

Figure 2.Working principle of an ALD process demonstrated by TiCl4 chemisorption on a hydroxylated surface followed by hydrolysis [104] - Published by The Royal Society of Chemistry.

A common film to be deposited via ALD is TiO_2, which can prepared from titanium tetrachloride and water precursors as shown in figure 2.

To deposit TiO_2, first titanium tetrachloride in its gaseous form is pulsed into the ALD chamber, where it begins to chemisorb on the substrate's activated surface until all possible location has been covered, thus completing the first 'half-reaction'. Followed by a purge with an inert carrier gas usually N_2 or Ar, to remove all of the remaining unreacted precursors and the undesired byproducts. Consequently, a hydrolysis pulse is initiated by introducing water vapor to the chamber, where the latter part of the 'half-reaction' is completed, and a monolayer of

TiO_2 has been deposited. Finally, N_2 or Ar gas is pulsed again into the chamber to remove both the unreacted H_2O and any byproducts [14]. This procedure is cycled until the desired film thickness is achieved, typically having a growth rate of 0.35-0.56 Å/cycle [15].

2.1.3 Physical Vapor Deposition

Physical vapor deposition (PVD) is a general phrase employed to represent many thin film deposition techniques, based on the condensation of the gaseous form of a solid material onto different surfaces [16]. However, dissimilar to CVD and ALD, PVD exploit the physical adsorption of a material to deposit atoms or molecules from the source to the substrate. This physical change is induced by either evaporation or sputtering, as shown in Figure 3. The deposition rates of PVD can vary between 0.1 to 100 nm/s [17].

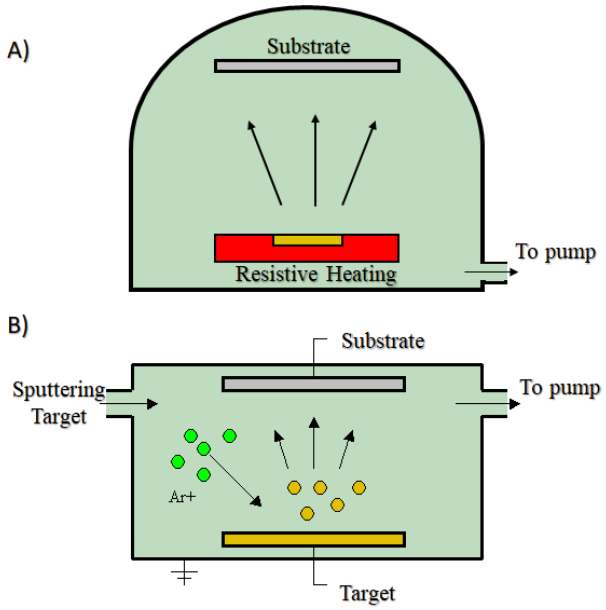

Figure 3. Physical Vapor Deposition types, A) Evaporative Deposition, and B) Sputtering Deposition. Images obtained from the Public Domain.

2.1.3.1 Sputtering PVD

Throughout the sputtering process, air within the chamber is replaced with an inert gas that is usually argon. Moreover, when a high voltage is applied, a glow discharge is commenced. The plasma originates from the collisions between the electrons and the argon atoms, wherein each electron strikes an argon atom ionizing it to an excited state of Ar^+ and releases an excess electron [10]. Nevertheless, the purple color of the glow is due to the recombination process between the excited Ar^+ ions and the electrons, which results in a photon release, as shown in the formulas bellow [18].

$$Ar + e^- \rightarrow Ar^+ + 2e^- \quad (2)$$

$$Ar^+ + e^- \rightarrow Ar + \gamma \quad (3)$$

Due to the applied electrical field, the energetic positively charged argon ions Ar^+ accelerate towards for the negatively charged target bombarding its surface. This results in an ejection of particles from the target, towards the substrate [19]. Nonetheless, an external magnetic field could be applied to better control the chaotic behavior of the energetic argon ions Ar^+ in a process known as magnetron sputtering [20].Lastly, introducing a nitrogen or oxygen gas to the reactor along with the argon gas would result in reactive sputtering, which is a method to sputter nitrides or oxides [21].

2.1.3.2 Evaporative PVD

Evaporating materials followed by condensation on a substrate is one of many techniques used to deposit thin films [22]. This process includes two phases of the material to be deposited, first being the condensed form whether it is in its solid or liquid, and the other being the vapor form. The evaporation of the material to be deposited is activated by thermal energy, where the vaporized/sublimated atoms or molecules are conveyed from the evaporation source to be later condensated on the lower temperature substrate. Thermal energy could be supplied in various forms such as (1) conventional resistive heating, where a metallic wire is heated as an effect of joule heating, (2) e-beam heating, where an electron beam is concentrated towards the evaporant, or via (3) a pulsed laser, where a high power laser is focused via lenses onto the target material [23]. Frequently, PVD is operated at ultrahigh vacuum conditions to minimize collisions and increase the mean free path of the atoms to be deposited, which would result in a uniform deposition [24].

2.2 Thermodynamics of evaporation

Typically, heating up any material to a temperature higher than its boiling point, causes the formation of bubbles. This phenomenon takes place due to the attained kinetic energy, supplied in the form of heat, which enables the materials molecules to overcome the intermolecular forces binding them to the condensed phase (e.g. Solid or liquid) [25], thus enabling them to leave the system as a vapor.

Furthermore, as more heat is supplied to the boiling material, a vigorous boiling is observed. Thus, with increasing temperature, higher kinetic energy is achieved, which sequentially satisfies the equation of kinetic energy of a gaseous particle mentioned bellow [26],

$$E_K = \frac{3}{2} k_B T \tag{4}$$

Where,

E_K is the kinetic energy,
k_B is the Boltzmann constant, and
T is the temperature in kelvin.

Conversely, the transformation of the materials from one physical phase to another (e.g. from liquid to vapor) can be explained by Gibbs phase rule, which predicts the effect of changing the temperature and pressure on a heterogeneous mixture [27].

The Gibbs phase rule can be written as:

$$F = C - P + 2 \tag{5}$$

Where,

F is the Degrees of freedom,
C is the Components of the system, and
P is the phases.

The above equation explains the degree of freedoms required to define the phase of a component, for example at the triple point of water (1 component system) where the 3 phases (Solid, Liquid, and Vapor) exist, F=0. Thus, both a specific temperature and pressure are required to identify the triple point as shown in the figure bellow.

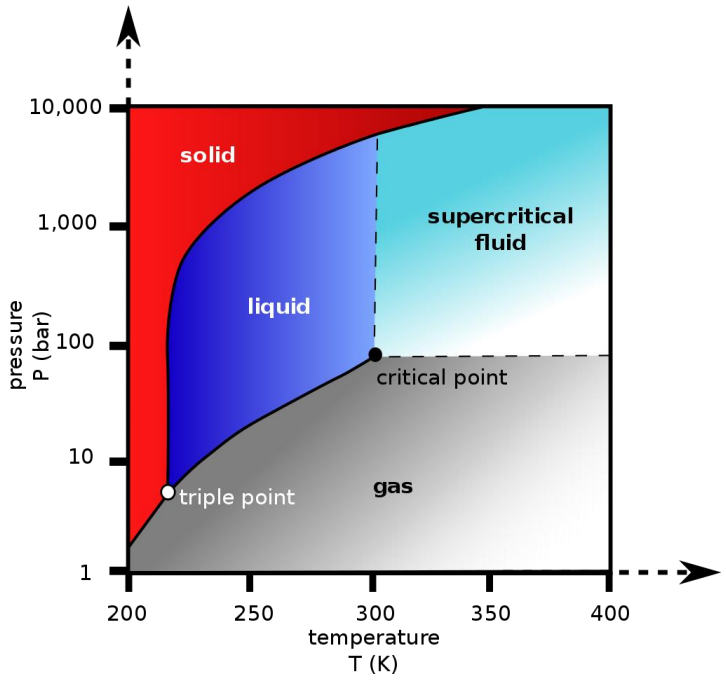

Figure 4. Carbon Dioxide pressure-temperature phase diagram

It should be noted that When the vapor pressure, which is a physical property of each matter, equals the hydrostatic pressure, that is the pressure acting on a material, boiling occurs. (E.g. hydrostatic pressure = atmospheric pressure, in an open system).

Therefore, not only the temperature of the system is the key requirement for the evaporation of the material to take place but also the pressure acting on the system plays a huge role in identifying the temperature of transformation from a liquid state to a vapor state, which is explained by the Clausius-Clapeyron relation expressed bellow.

$$\ln\left(\frac{P_2}{P_1}\right) = -\frac{\Delta H_{vap}}{R}\left(\frac{1}{T_2} - \frac{1}{T_1}\right) \quad (6)$$

Where,

P is the Pressure,
R is the Universal Gas Constant,
ΔH_{vap} is the Latent heat of Vaporization, and
T is the Temperature.

The Clausius-Clapeyron relation explains the dependent relationship between the vapor pressure and the temperature. Furthermore, it is important to identify the temperature required to archive a specific vapor pressure [17]. A graphical representation of the dependency of vapor pressure on temperature is shown in Figure 5.

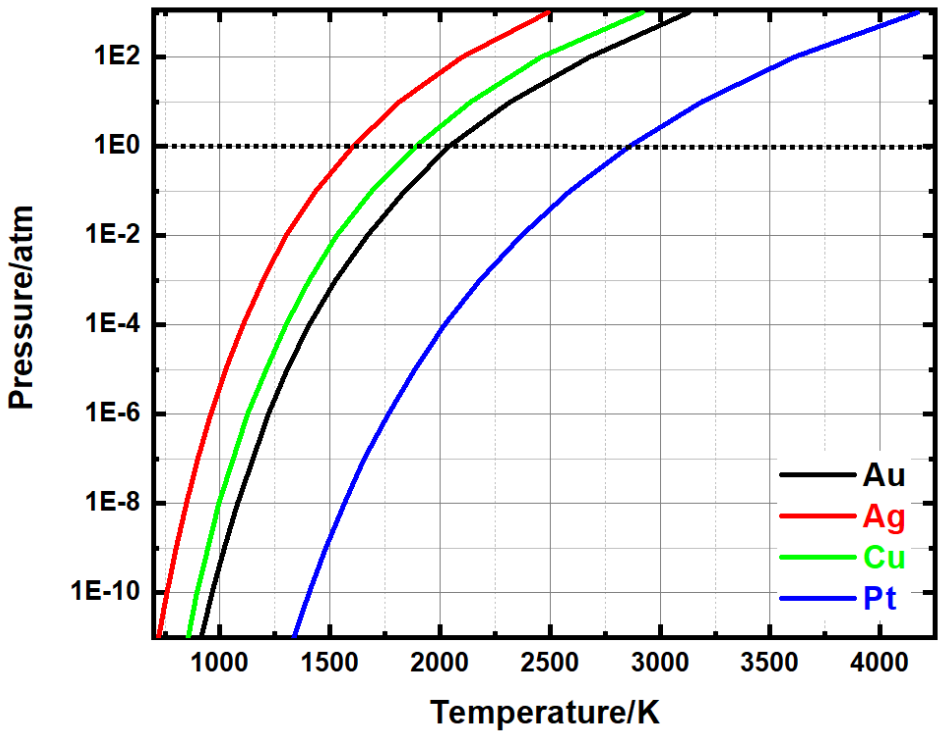

Figure 5. Vapor Pressure of multiple metals as a function of temperature [98].

So that with decreasing the hydrostatic pressure that is acting on the material through the means of vacuum pumps, lower temperature is needed to for the phase transition from liquid to gas.

2.3 Evaporation Profile and Film Uniformity

As the material is being evaporated, its evaporation profile is dependent on the source's geometry. Langmuir evaporation explains the evaporation from a free surface [28], while effusion describes is the evaporation through an orifice. Decreasing the size of the evaporation source, results in a more oriented evaporation profile, as shown in figure 6. Narrower evaporation profiles are very much appreciated hence, it would result in less deposition on the evaporator walls, which in turn would reduce contamination and costs.

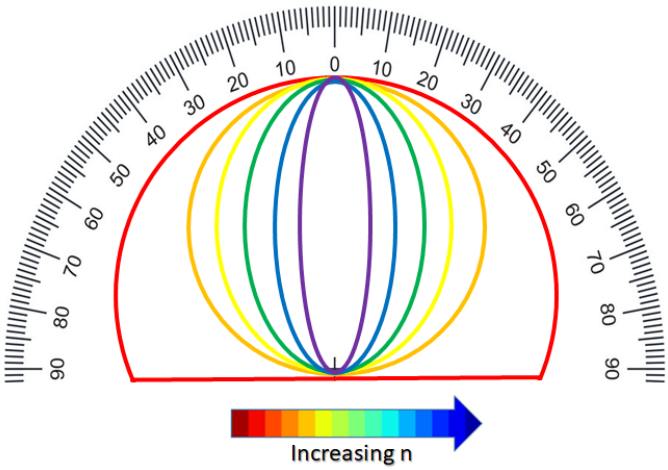

Figure 6. Graphical representation of the different evaporation profiles, as a function of cosine exponent

2.3.1 Cosine Law

The evaporated atoms from a source always follow a directional evaporation profile, thus the angle and the distance between the source and the substrate are extremely important to maintain a uniform film with minimum flouting. The deposition of the evaporated species can be controlled via the cosine law [23].

$$\frac{M_s}{A_s} = \frac{M_e(n+1)cos^n\phi cos\theta}{2\pi r^2} \quad (7)$$

Where,

$\frac{M_s}{A_s}$ is the Mass deposited per unit area,
M_e is the Evaporated Mass,
n is Geometric factor,
r is the Distance from the source to substrate,
ϕ is the angle between the source and substrate, and
θ is the Angle between the normal and the source.

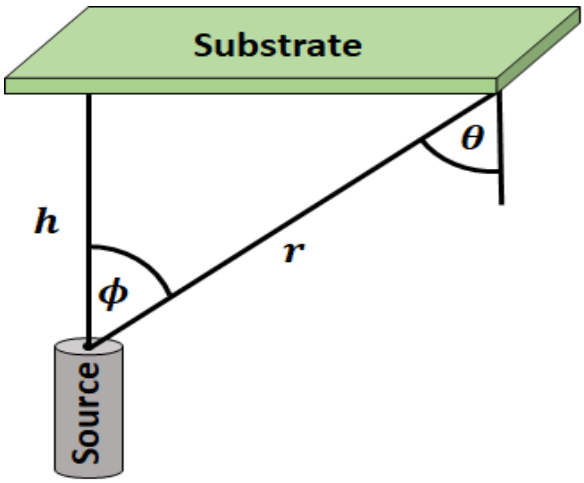

Figure 7. Visual Representation of the cosine law [100].

The value of the geometrical factor, n, can be determined by the evaporation source structure. For an extended surface source n has the value of 1, furthermore as the source's size decrease, the n value increases, which results in a more directional evaporation profile as shown in Figure 6.

2.3.2 Evaporation rate

At any surface with a lower temperature than the surrounding, is preferable medium for the condensation of the vapor molecules. The condensation occurs at a rate controlled by the pressure, temperature and the mass of the evaporated atoms, also known as the Hertz-Knudsen Equation [29, 30] shown below.

$$\Phi = \frac{\alpha_e (P_v - P_c)}{\sqrt{2\pi m k_B T}} \tag{8}$$

Where,

Φ is the Evaporation flux of the gas molecules,
α_e is the Evaporation coefficient,
P_v, P_c is the vapor and chamber pressure respectively,
m is the mass,
k_B is the Boltzmann constant, and
T is the Temperature.

The above equation is crucial to determine the rate at which the film is growing [17].

2.3.3 Film Growth and Wettability

Indeed the evaporated species would tend to form a film on the cooler substrate, yet between the first contact and the final deposited film, lays many stages that can be observed in figure 8.

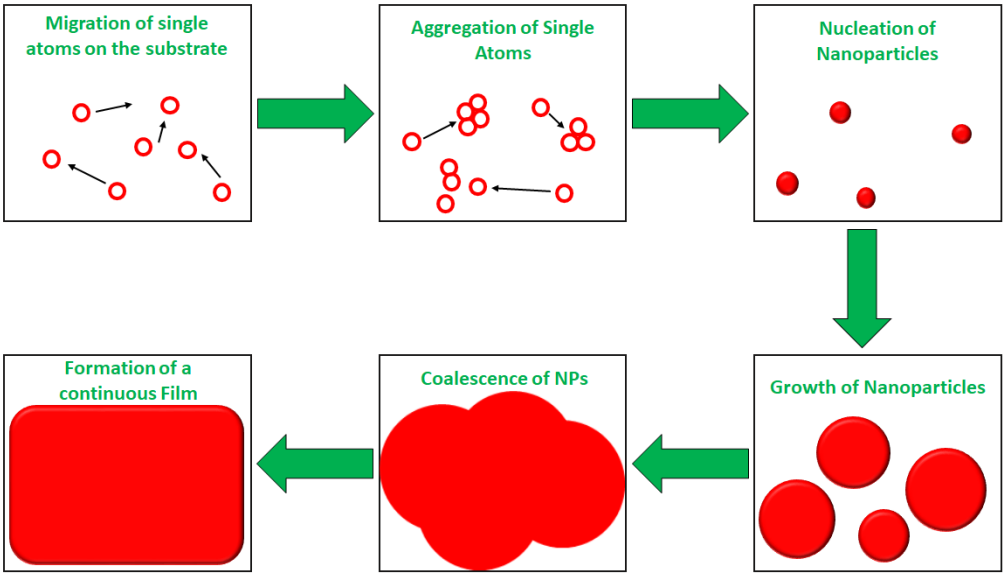

Figure 8. Stages of a continuous film formation

The formation of a film starts with the adsorption of the evaporant atoms on kinks, dislocations or contamination on the substrate surface. In addition, single evaporant atoms would tend to migrate on the surface combining with other evaporant atoms to reduce their surface energy, thus the aggregated atoms start forming clusters. Subsequently, these clusters would act as nucleation points for further growth. As the nanoparticles grow bigger and bigger in size, they would start to merge with one another, until finally a continuous film is formed. Finally, further growth would result to an increase in the film thickness.

When the evaporant encounters a solid surface, a contest between the adhesive and cohesive forces commence. The adhesive forces between the solid surface and the evaporant, attempts to spread the material on the entire surface, while the evaporant intermolecular forces, cohesive forces, would tend to keep the evaporant particles together minimizing its surface energy. Reliant on which force prevails, the surface would either be wetted or not, respectively.

Thomas Young was the first to document this phenomenon [31], which resulted in his relation shown below,

$$\gamma_{LV}\, cos\theta = \gamma_{SV} - \gamma_{SL} \tag{9}$$

Where,

γ_{LV} is the surface energy between the fluid and surroundings,
θ is the Contact angle,
γ_{SV} is the surface energy between the substrate and surroundings, and
γ_{SL} is the surface energy between the substrate and fluid.

The surface wettability decides the growth mechanisms of the continuous film. Theses growth routes are divided into 3 types, first being when the surface is completely wetted by the fluid, which initiate (1) the growth of smooth films also known as Frank -van der Merve layer-by-layer growth. Controversially, when the surface is not wetted by the fluid, (2) a growth of rough patchy films is preferred known as Volmer–Weber Island growth. Finally an intermediate phase that both (3) layer and island growth are favored, known by Stranski-Krastanov layer-plus-island growth mode. [32]

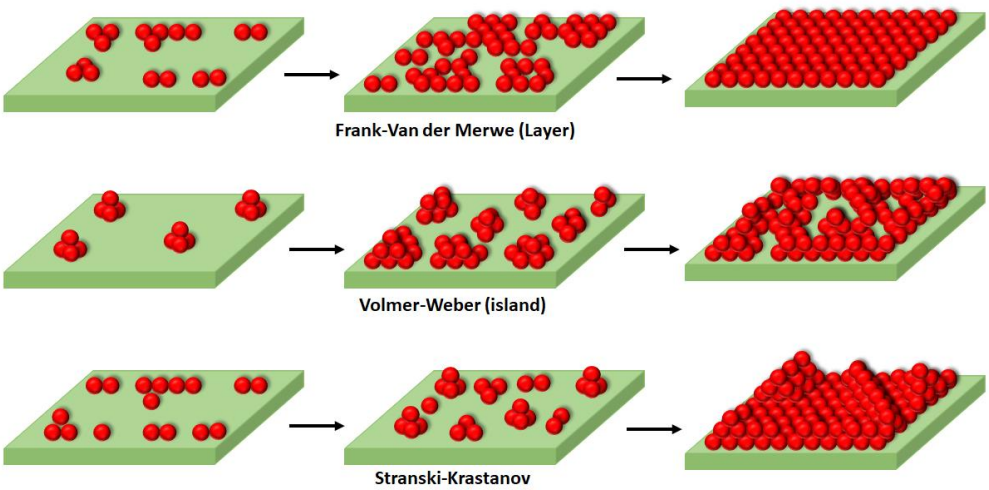

Figure 9. 3D sketch of the three primary modes of thin film growth. [101]

Referring back to equation 6, when surface energy of Substrate-Surroundings equals the surface energies of both Substrate-Fluid and Fluid-Surroundings, $\gamma_{SV} = \gamma_{SL} + \gamma_{LV}$, layer growth is favored.

For island growth, the surface energy of Substrate-Surrounding should be smaller than the sum of the other two surface energies, $\gamma_{SV} < \gamma_{SL} + \gamma_{LV}$.

Nonetheless, when the surface energy of Substrate-Surrounding is larger than the sum of the other two surface energies, $\gamma_{SV} > \gamma_{SL} + \gamma_{LV}$, which in turn results in both mechanism layer and island combined.

2.4 Thin films

A thin film is a general term, describing a layer of a material with a thickness ranging from a one atom thick to several micrometers [33]. Thin films has been attractive to many fields due to their remarkable properties that differ from their bulk counter forms.

2.4.1 Thin films and bulk materials

Due to the reduced thickness and the increased surface area, unusual physical phenomena are attained by thin films such as, electron scattering from surface, nonlinear diffusion, and quantum effects [34]. These phenomena gives rise to thin films properties that does not only mismatch with their bulk counterparts but also dependent on the film thickness and the deposition method in some cases. These properties include density, resistivity, dielectric constant, coefficient of thermal expansion, and refractive index [35].

2.4.2 Thin films via evaporative deposition

Many materials such as metals [36], ceramic [37] and polymers [38] can be evaporated and deposited as thin films using evaporative deposition technique. These films can be implemented in a diverse set of application fields such as in mechanical [39], electrical, [36] energy [40] optical [41], medical applications [42, 43].

2.4.2.1 Metals, Compounds and alloys

Metals evaporate as atoms or seldom cluster of atoms, however very few compounds evaporate similar to metals where their vapor composition is identical to their bulk counterpart [23]. There are three main reaction types in which compounds to be evaporated can follow, these reaction types are summarized in table 1.

Evaporation without dissociation	$MX_{(s\ or\ l)} \rightarrow MX_{(g)}$	SiO, SnO,AlN
Decomposition	$MX_{(s)} \rightarrow M_{(l)} + \frac{1}{n} X_{n(g)}$	Ag_2S, Ag_2Se III-V Semiconductors
Evaporation with dissociation	$MO_{2(s)} \rightarrow MO_{(g)} + \frac{1}{2} O_{2(g)}$ (oxides)	SiO_2,GeO_2,TiO_2

M = metal, X= nonmetal. *X = S, Se, Te.

Table 1.Thermal evaporation of compounds reaction types [44].

Evaporation of alloys on the other hand, is much more complicated, since each component would exhibit a different evaporation profile, and will tend to be evaporated independently [45]. To overcome the aforementioned difficulty many solutions has been suggested to achieve the desired film composition, such as changing the source material alloy composition percentage while considering the interaction energy among the alloy's material components, or via utilizing two sources of materials in a process known as co-deposition.

2.4.2.2 Polymers and organic compounds

Unlike metals, which are distinguished by their metallic bonds, organic materials are bounded via intramolecular covalent bonds and intermolecular forces such as weak van der Waals, hydrogen bonding or dipole-dipole interactions.

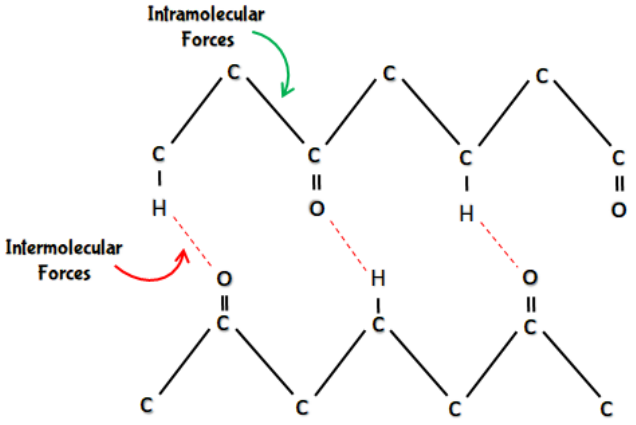

Figure 10. Inter and Intra molecular attraction between two carbon chains.

Naturally, covalent bonds energy varies between 2-5 eV, while van der waals and hydrogen bonds are much more weaker 0.01eV, and 0.1-0.4 eV, respectively [46].

Evaporative deposition technique uses thermal energy to overcome the intermolecular forces, without effecting the integrity of the molecule by breaking its intramolecular attractions.

2.5 Organic photochromic molecules

In 1950, Hirshberg set a new term [47], which is derived from the two Greek words: *phos* (Light) and *chroma* (Color). The term photochromism imply defines the reversible light-activated change of color [48].

2.5.1 Kinetics

When exposed to specific electromagnetic radiation organic photochromic molecules absorb the radiation to exhibit either isomerization (e.g. trans-cis / cis-trans), or result in a ring opening /closure [9]. In both cases, the resultant is a metastable state of the molecule that has a shifted absorbance peak as displayed in figure 11.

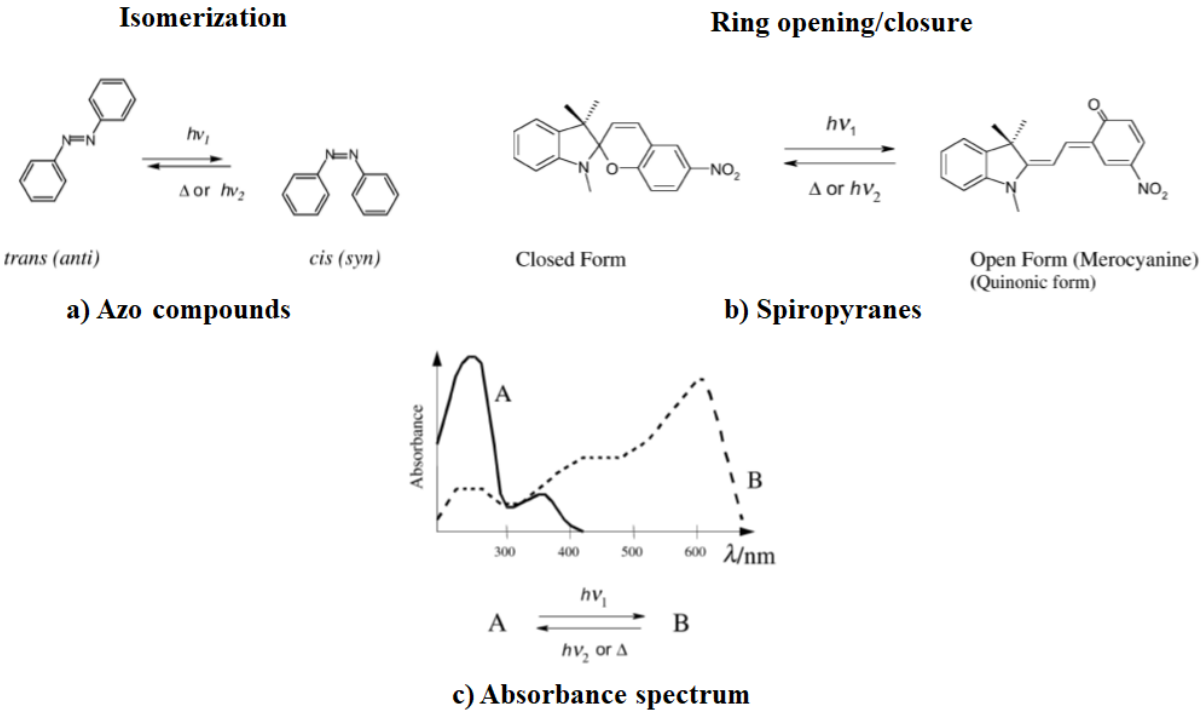

Figure 11. Types of organic photochromic molecules, where $h\nu_1 > h\nu_2$ and Δ represents temperature. a) Azo Compounds that show isomerization, b) Spiropyranes, which exhibits ring opening/closure, and c) the absorbance curve, which shows the absorbance speak shift between the closed state A, and the open state B. [48] ©IUPAC 2001

The two isomers, the initial state and the metastable state, not only differ in their absorption spectra, but also they differ in many physical and chemical properties such as geometrical structures, dielectric constants, refractive indices, and oxidation-reduction potentials [49]. Predominantly most organic photochromic molecules are either colorless or pale yellow before UV illumination and are colored in their metastable phase, in a process called positive photochromism. On the other hand some molecules demonstrate negative photochromism, in which are colored in their stable form and are colorless in their metastable state [48].

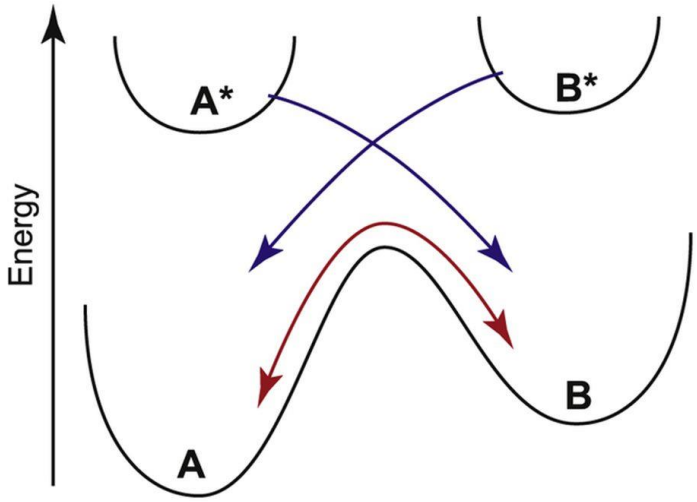

Figure 12. Two photo-isomers, converting from the stable state A to the excited state B. Blue lines indicate conversion via light, and red arrows indicate conversion via thermal energy [50].

When isomer A is exposed to stimuli I, Figure 12, it transforms into an intermediate state A^* which then decays back to the metastable state B in a time interval of picoseconds [51]. Similarly, when the metastable state B is subjected to stimuli II, it transforms into an intermediate state B^* before decaying to the thermodynamically most stable state A [52].

2.5.2 Types

Type	Definition	Example
Photochromic	Electromagnetic radiation activated transition	Spirooxazine Azobenzene
Thermochromism	Thermally activated transition	Spirooxazine Bianthrones
Solvatochromism	Solvent activated transition	Spirooxazine Reichardt's dye
Acidichromism	Proton H^+, or hydroxyl OH^- activated transition	Spirooxazine

Table 2. Types of chromism [53].

2.5.3 Colorability and Degradability

The ability of a photochromic molecule to transform from a bleached to an activated isomer is known as colorability. The colorability of a photochromic molecule is directly linked by the quantum yield of the molecule that describes the efficiency between the number of photon

absorbed and the number of photons that were supplied [50]. Nonetheless, photo-isomerization is a nondestructive method, yet photochromic molecules are vulnerable to unwanted side reactions such as oxidation that causes degradation in a process known as fatigue [54].

2.5.4 Spirooxazine

Spiroxazine (SO) was a vital contributor to revive the activity of organic photochromic molecules in research and markets due to its fatigue-resistant property [55]. When exposing Spirophenanthroxazine (SPO) to UV irradiation, it experience a reversible cleavage of the spiro C-O bond that is located at the oxazine ring. Furthermore, the molecule's two part, indoline and phenanthooxazine, then twists to form the final planer photomerocyanine (PMC) form, Figure 8. Due to the rotation, and the double bonds between the indoline and phenanthooxazine sides, eight possible isomers can exist [56]. SPO is a photo-, thermo-, solvato-, and an acidichromic molecule, accordingly upon exposing the PMC form to white light radiation, or heat the molecule can revert to its closed SPO form.

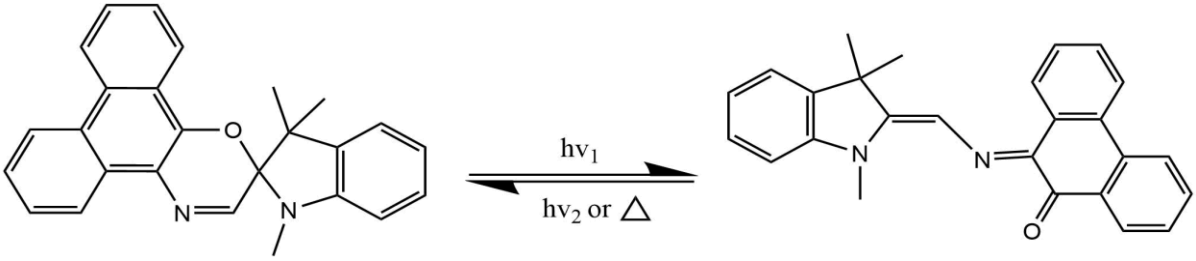

Figure 13. Left: Closed form of SPO (left), and its PMC form (right), where $hv_1 > hv_2$ and Δ represents temperature.

2.5.4.1 Applications

Due its sensitivity towards light, heat, solvents and acidity stimuli, SO has become an interest to both the scientific and industrial communities possessing a widespread of applications including the fields of chemical sensing [57] [58] rewritable data storage [59] [60] , optical devices [61], smart windows [62], and many other modern applications [63] [64]. Among these applications, Hongyan and his group presented a liquid-state chemical sensor that is selective and sensitive to cyanide anions [65]. While, Paird presented a study on the solvatochromic decay of spiropyran in several organic liquids such as acetonitrile, toluene, and THF [66]. Lastly, In 2011 Jamali, Mohammad, et al. revealed the first proof of concept experiment where they exposed a thin film composed of SPO in embedded in Polystyrene (PS) matrix to multiple volatile organic compounds, wherein they observed an extremely accelerated bleaching effect as compared to thermal and photo bleaching. They suspected that the accelerated bleaching is an effect of the expansion of the PS matrix, which facilitates the way for the reverse switching of SPO [67]. It's worth mentioning that the aforementioned film was produced by spin coating

method, where the need of a viscos media is a necessary for the deposition process to take place, in consequence SPO molecules can not be deposited without a supporting matrix.

In this work, with the aid of vacuum thermal evaporation technique, standalone SPO molecules with various surface features were deposited on multiple substrates without any supporting matrix. These molecules were also tested under the influence of multiple volatile organic compounds to analyze their sensing mechanism and properties.

3 Materials and Methods

3.1 Materials

Within this work, the photochromic molecule 1,3,3-trimethylspiro[indoline-2,2'-phenanthro[9,10-b][1,4]oxazine] (CAS no. of 119980-36-8, purity >98%, Hangzhou Sage Chemical Co. Ltd., China.) was used and its structure is given in figure 12. Acetone, Acetonitrile, and isopropanol, ACS reagent grade obtained from Sigma Aldrich were also used in this work as part of the sensor study. 2x2 cm^2 laboratory grade glass slides with thickness of 1mm, Silicon (Si) wafers and SiO_2 /Si (1.5µm thick SiO_x) wafers, were used as substrates for the deposition process. All substrates were cleaned via technical grade acetone and isopropanol. Moreover, all chemicals were used as received, without any further purification. It should be noted that, the silicon wafers used in this work still possess their native oxide layer but are they are referred as Si substrates in this work for simplicity.

3.2 Film Deposition

3.2.1 Vacuum Evaporation Chamber

The film deposition took place in a vacuum chamber, figure 13, constructed by the institute for materials science at CAU, Kiel. The designed vacuum chamber can achieve ultrahigh vacuum of 10^{-9} mbar, via the assistance of two independent pumping systems. A rotary pump, Adixen APC 28/40 by PFEIFFER vacuum, system that achieves a pressure of 10^{-2} mbar passivating the way for a more powerful turbo molecular pump, HiPace 300 by PFEIFFER vacuum,

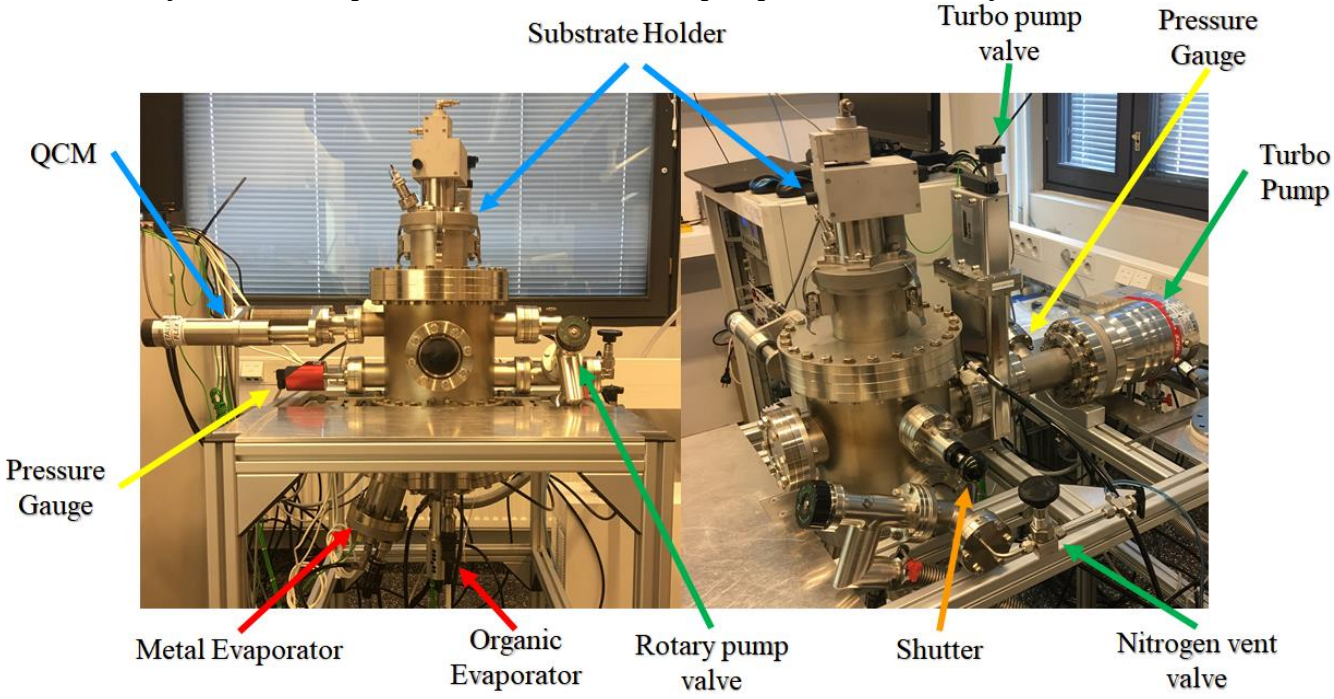

Figure 14. Vacuum thermal evaporator chamber components.

system. Within the vacuum chamber, the substrate holder temperature can be controlled via external closed loop cooling/heating circulating system. Having such thermostatic deposition control allows the deposition of thin films at temperatures ranging from 1°C - 90°C (incase of water coolant). Moreover, with an implemented rotary motor, the deposition stage has the ability to spin ensuring more uniform film deposition.

An ORganic MAterials (ORMA) evaporator supplied by Mantis Deposition Ltd. is mounted within the chamber. ORMA contains six pockets that can be loaded with 60 mm^3 quartz crucible. Each pocket can be heated up to 600°C independently via DC filament heating. The temperature of the quartz crucible is measured using a k-type thermocouple and can be controlled via the MANTIS software.

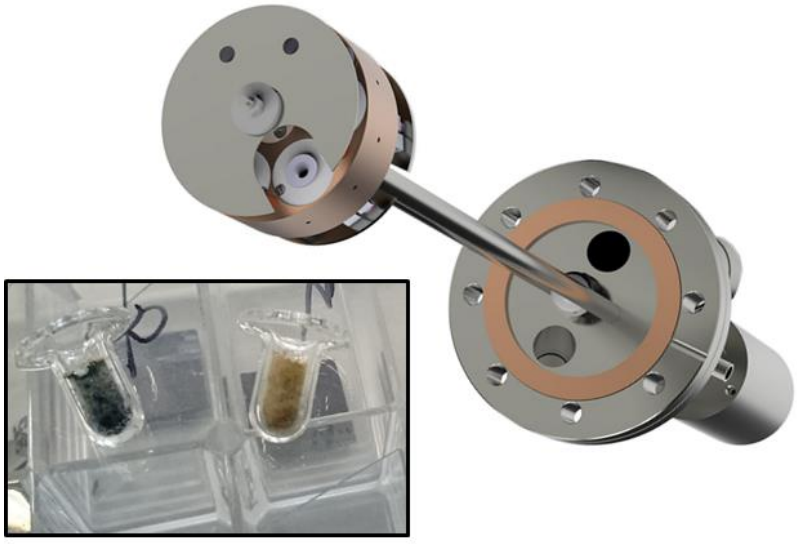

Figure 15. Organic Materials (ORMA) Evaporation source, and the 60mm^3 quartz crucibles.

Finally, to monitor the evaporation rate and the film thickness, a Quartz Crystal Microbalance (QCM) system is mounted parallel to substrate holder. The QCM has an oscillation frequency of 6 MHz and is provided by Inficon, USA. Moreover, the data received from the QCM, and the k type thermocouple is processed via a film thickness monitor, EON-LT, and displayed using an EON software both supplied by Colnatec.

3.2.2 Film deposition parameters

Laboratory grade glass, Si, and SiO_2 /Si Substrates were cleaned using Acetone and isopropanol, the substrates were then dried via an air gun and were placed in a cleaned, dust-free box.

10mg of Spirophenanthrooxazine (SPO) powder were loaded in a quartz crucible; the powder was mixed with 50 µl of isopropanol, which resulted in a muddy form of the SPO for an easier control while compressing the powder into the crucible.

The cleaned substrates were attached to the thermal evaporator substrate stage, and placed into the chamber along with loaded quartz crucible. The substrate stage was then connected to the water circulation system, which was kept at 20°C. As the pressure within the chamber approaches the value of $5x10^{-6}$ mbar, the temperature of the thermal evaporator was set to increase gradually to a final temperature of 140-145°C. When the temperature and the deposition rate stabilized, the evaporator shutter was opened and the deposition was initiated. The deposition rate for both continuous films and percolated samples was ~1.3Å/s, while for the particle sample was ~0.7 Å/s. Once the desired thickness was achieved, the shutter was closed, and the procedure was terminated.

Finally, as the temperature of the thermal evaporator approached room temperature, the chamber was vented using nitrogen and the substrates were recovered and placed in a black box (opaque) container.

3.2.3 Film activation

As mentioned earlier, exposing the SPO to radiation promotes the transformation from one form to another. In this work both a 365 nm UV source, H135 UV 35W, and a White lamp, H135 WH 35W, supplied by Labino® were used at a distance of 18 cm from the sample. The irradiance of the UV source was 0.2 $W/cm^{2,}$ while the intensity of the white light was 48.2 Mcd. The samples were illuminated initially with UV radiation followed by iterative cycles, consisting of an exposure to visible light tailed by another UV radiation exposure. The exposure times for the continuous films were 3 minutes under UV radiation, and 2 minutes under white light. While for both the percolated and particle samples the exposure times were 2 minutes under UV radiation and 1 minute under white light.

3.3 Material Characterization

3.3.1 Composition and Structure

3.3.1.1 Nuclear Magnetic Resonance Spectroscopy

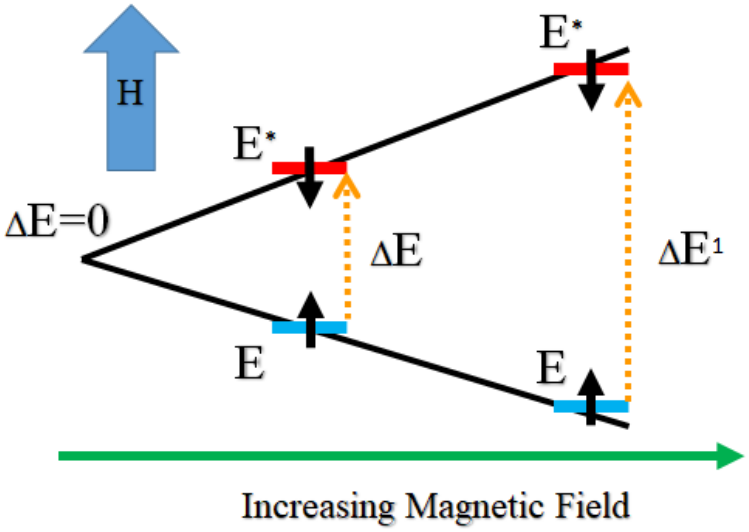

Figure 16. Illustration of the working principle of NMR, the blue arrow indicates the direction of the magnetic field, blue and red lines represent the ground and excited states respectively.

Nuclear Magnetic Resonance (NMR) Spectroscopy is a method used by organic chemists to identify the molecular structure of on organic molecule. NMR working principle relies on the nuclei, which contain an odd number of protons, such as H^1 and C^{13}. Typically, nuclei with an odd number of protons possess a nuclear spin however; under normal conditions, these spins are disordered. When subjected to a high magnetic field, these spins would tend to arrange themselves parallel with the employed field either aligned or opposing, Figure 15. The energy required to flip the spin from aligned to opposing or vice versa, lays in the radio frequency range [68]. Thus, when exposing the sample to radio waves, some of these waves are absorbed, depending on location and surroundings of each nuclei, taking an atom from a ground state into an un-favored excited state, which tend to reemit the absorbed radio wave. Based on the absorption and emittance of radio waves, a distinctive spectrum for each molecule could be obtained.

In this work ^{1}H- NMR and ^{13}C-NMR spectra were recorded with a Bruker AVANCE 400 MHz spectrometer by Bruker with a 5 mm BBFO probe. 10 mg of SPO was dissolved in (1) deuterated Dimethylsulfoxide (DMSO) and (2) Deuterated Chloroform ($CDCl_3$) as the solvents. The chemical shifts were presented in ppm downfield using tetramethyl silane (0 ppm) as an internal standard.

3.3.1.2 Differential scanning calorimetry

Differential Scanning Calorimetry (DSC) is a technique to observe the response of polymers to the supplied heat. Its working principle depend on supplying two heating plates with an identical heating profile, where the first contains the sample and the other is an empty reference. The difference between the heat flow of the sample and the reference is recorded and plotted verses temperature or time. Depending on the amount of heat flow the data describes both the

endothermic (e.g. melting) and exothermic (e.g. crystallization) reaction occurring within the sample [69].

In this work, the thermal analysis was preformed via DSC 6000 provided by PerkinElmer. ~10mg of the SPO powder was investigated against an identical empty reference sample. The heat flow was recorded under nitrogen atmosphere, from 30°C to 250°C, and then back to 30°C at 20.00°C/min.

3.3.1.3 Fourier-transform infrared spectroscopy

Fourier-transform infrared spectroscopy (FTIR) is an important technique to identify a sample's molecular and structural properties. FTIR spectroscopy works by exposing the sample to the infrared region of the electromagnetic spectrum, which is in turn absorbed. The absorption of infrared radiation is translated to the vibration and stretching of the molecules within the sample [70]. The data received from the FTIR spectroscopy is interpreted as transmission or absorption vs wavenumber (frequency).

In this work the infrared spectra of the SPO powder, and the SPO deposited film on silicon wafer was recorded by ALPHA II FTIR spectrometer by Bruker using attenuated total reflection (ATR) mode. Each sample scan's number was set to be 48 scans, and the data was recorded from 4000 cm^{-1} to 500 cm^{-1}.

3.3.1.4 Grazing Incidence X-Ray Diffraction

Grazing Incidence X-Ray Diffraction (GI-XRD), just as a conventional XRD device is a technique that provide information such as lattice parameters, crystal structure and crystallinity using the angle of diffraction of X-rays from the sample. X-ray are used because of their wavelength of 1Å, which makes them suitable for the interatomic spacing between atoms. Due to the interaction between the sample's interatomic spacing and the subjected X-rays, diffraction occur in respect to Bragg's law, where the diffracted X-rays are either constructive or destructive and are read by the detector [71]. However, unlike XRD, GI-XRD uses small incident angles where the beams do not penetrate deep into the sample, but rather provide surface information. This feature promotes GI-XRD to be a suitable candidate for thin films characterization.

In this work the crystal structure of the deposited films were analyzed by X'Pert Pro Alpha 1 MPD supplied by PANalytical. The X-rays patterns were recorded at 2θ intervals between 5°

and 90° at step size of 0.050° using Cu K_α radiation operating at λ= 1.540598 Å, 40 kV tube voltage and 40mA current. Moreover, the system was pre-calibrated prior to the measurement.

3.3.2 Thickness and morphology

3.3.2.1 Profilometer

Similar to atomic force microscopy AFM, the profilometer uses a stylus to scan over a 2D surface. This technique is used to identify the samples surface topology; moreover, it is widely used as a tool to identify the thickness of the deposited film. [72]

The deposited SPO film thickness was determined via DekakXT profilometer by Bruker. A standard scan profiling hills and valleys using a 12.5 μm radius stylus at 10 mg force was performed on a scratched SPO film on a glass substrate. Multiple locations on the film were measured and a mean value was obtained.

3.3.2.2 X-Ray Reflectometry

X-Ray Reflectometry (XRR) is a nondestructive tool that is used to study thin films' thickness', densities, interfaces and surface roughness. Its working principle relies on the specular reflections of a monochromatic x-ray from a thin film's surface, which obeys Fresnel law of reflectivity. XRR function around a critical angel, in which x-rays penetrate slightly into the thin film. However, above the critical angel the x-rays penetrate deeply into the substrate where the reading are no longer valid [73].

In this work the deposited films thickness, density and surface roughness were analyzed via X'Pert Pro Alpha 1 MPD manufactured by PANalytical. The X-rays patterns were recorded at 2θ-Ω intervals between 0.45° and 2.502° at step size 0.006° with Cu K_α radiation operating at λ= 1.540598 Å, 40 kV tube voltage and 40mA current. Moreover, the system was pre-calibrated prior to the measurement.

3.3.2.3 Scanning Electron Microscope

Scanning electron microscope (SEM) is an important tool to study the materials morphology and surface topology. SEM utilize accelerated electrons emitted from an electron gun towards a conductive sample, these electron will then interact with sample in two main forms that are useful for imaging [74]. The first interaction is the generation of secondary electrons (SE), in which an accelerated electron knocks off an outer shell electron of the sample, while the latter is the back scattered electron (BSE), in which the same accelerated electron is deflected by

the positive nucleus of the sample. Imaging in SE mode is a useful technique to observe the sample topology, while BSE mode is more favorable in identifying different phases and compositions within the sample. [75]

The SEM images are conducted using a Tuscan Mira3 SEM at different magnifications. The deposited films on both Si and SiO_2/Si wafers were investigated to obtain the deposited SPO morphology and percolation. The images were taken at an accelerating voltage of 5kV-6kV, a working distance of 10 mm, and using an In-Beam secondary electron detector.

3.3.3 Optical Characterization

3.3.3.1 Ellipsometry

An ellipsometry is a non-invasive method to examine thin film from a single angstrom thickness up to few micrometers. The ellipsometery provides information such as the film thickness and coverage, as well as the optical constants such as the refractive index. Its working principle relies on the interactions between a polarized light and the sample; moreover, the extracted data is then fitted into models to be interpreted. [76]

The optical constants and a film thickness map were acquired using M-2000 ellipsometer from J.A. Woollam Co., Inc. The data was recorded at multiple angels between 65 to 75, moreover CompleteEASE program also provided by J.A. Woollam was used to record and fit the attained data.

3.3.3.2 UV-VIS Spectroscopy

Ultraviolet-Visible (UV-VIS) spectrophotometer is a vital tool in determining the excitation energies of electrons of a sample. Typically, a UV-Vis spectrophotometer exposes a sample and its reference to multiple monochromatic wavelengths scanned from the UV-C region 200nm up to the near infrared radiation (NIR) region of 800nm. Simultaneously, the UV-Vis spectrometer records the interactions, absorption, reflection and transmission, between the electromagnetic spectrum and the sample. This technique can be utilized to measure the band gap, and to determine sample's concentration in accordance to Beer-lambert law. [77]

In this work, the UV-Vis spectra were obtained via UV-2600 with ISR-2600Plus Integrating Sphere Attachment supplied by Shimadzu. The transmission and absorption spectra of the deposited thin films were obtained from 800 nm to 350 nm against a reference glass substrate using a film holder (P/N 204-58909) designed for thin films. In addition, the relative specular reflectance spectra of the aforementioned thin films were obtained at incident angle of 8

degrees from 800nm to 350nm against a reference aluminum mirror using integrating sphere attachment.

3.3.3.3 Optical Microscope

An optical microscope is a tool to observe the microstructures of various materials using a set of lenses and the visible part of the electromagnetic spectrum. When the sample is placed next to the objective lens, visible light rays coming from the sample forms an inverted magnified image between the objective and the projected lens. Subsequently, the light rays from the developed inverted image are then converged by the projector lens leading to a final magnified image. [78]

The optical images at multiple magnifications of the freshly deposited and the aged SPO films on glass substrates were taken via ZIESS AXIO light microscope equipped with an AXIOcam 503 color camera. The focus was tuned in accordance to the sample height and the light intensity was adjusted to achieve the highest contrast. Moreover, the images were then modified by ZEN 2.3 software also provided by ZIESS.

3.4 Solvato-bleaching measurements

3.4.1 Vacuum Chamber

The gas phase sensing measurement were conducted in a vacuum chamber figure 16, which was constructed by the institute for materials science at CAU, Kiel. The designed vacuum chamber can achieve rough vacuum of 1.2 mbar, through the assistance of a scroll pump, nXDS6i by Edwards Vacuum. For the measurement, a 2x2 cm^2 sample holder mounts on a water circulated sample stage, which allows conducting experiments at various temperatures ranging from 5°C- 40°C. A Duran bubbler bottle is connected to the vacuum chamber allowing the introduction of numerous volatile compounds. Moreover, a UV-Vis-NIR spectrophotometer system is connected to the chamber, the system consists of (1) a UV-Vis-NIR light source, DH-200-BAL by Ocean Optics, providing a broad range of the electromagnetic spectrum by using Deuterium and Halogen lamps, and (2) a CCD array spectrometer, HR4000CG-UV-NIR by Ocean Optics, that detects wavelengths ranging between 190-1100 nm. The spectrometer is connected to OceanView software, supplied by the

same manufacturer. Both the light source and the spectrometer are connected via fiber optics, QP400-2-SR-BX by Ocean Optics, which disconnect at the sample location.

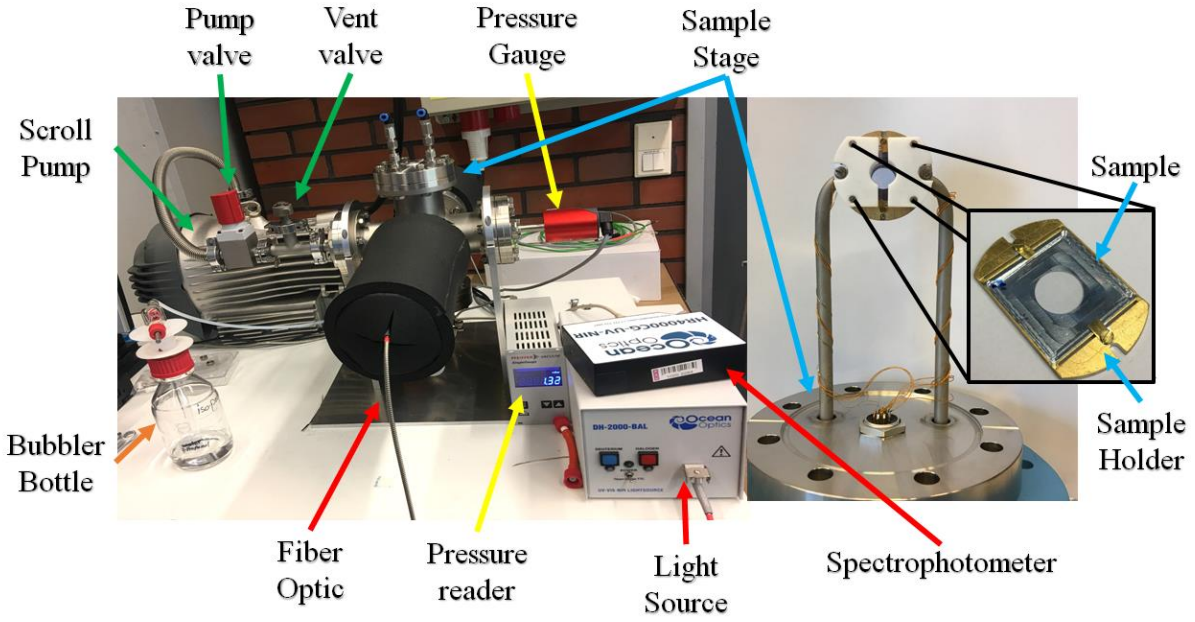

Figure 17.Gas-Phase sensor components.

3.4.2 Time-Resolved absorption measurements

Prior to the conductance of any experiment, the UV-Vis spectrometer was background corrected. UV illuminated samples of SPO on glass substrates were placed in the sample holder and into the vacuum chamber, where the initial pressure was 1.3mbar throughout all experiments. A maintained 100ml of DI water, acetone, acetonitrile and isopropanol liquids were filled in different Duran bubbler bottles that were connected to the chamber. When the bubbler valve was opened, the pump valve was successively closed allowing the pressure buildup of the gas within the chamber and simultaneously, initiating the acquisition of the absorption spectra. Table 3 summaries the initial pressures, constant pressures, final pressures and the acquisition times of the deposited SPO films for all 4 chemical compounds used. After the exposure of the gas, the film was extracted to be illuminated under UV radiation for the following experiment.

Film type	*Liquid type*	*Constant Pressure(mbar)*	*Acquisition Start pressure (mbar)*	*Final Pressure(mbar)*	*Acquisition (msec)*	*Time (min)*
Continuous film	Water	7	7	29	500	1
	Acetone	28	28	186	500	1
	Acetonitrile	34	34	91	500	1
	Isopropanol	6	40	54	1000	2
Percolated sample	Water	7	7	29	500	1
	Acetone	28	28	186	500	1
	Acetonitrile	34	34	91	500	1
	Isopropanol	6	40	54	500	2

Table 3. The acquisition parameters of the Gas-phase sensor experiment for both the continuous and percolated samples.

The above table describes the following:

- Constant Pressure: the pressure after opening the bubble valve and before closing the pump valve.
- Acquisition pressure: the pressure at which the reading commence.
- Final pressure: the final value of build up pressure.

4 Results and Discussion

As mentioned earlier in chapter 2, Spirooxazine photochromic molecules has been utilized in many applications, moreover these molecules have been deeply investigated using time-resolved spectroscopy at micro- [79], pico- [80] and femto-second [81]. Spirooxazine molecules would tend to form a metastable state as a response to stimuli, wherein the excitation and relaxation occur at very fast rates for diluted samples. It has been reported that spirophenanthrooxazine has a thermal decoloration rate constants of 1.1 s^{-1} and 2.4 s^{-1} in acetone and acetonitrile solvents, respectively [79].

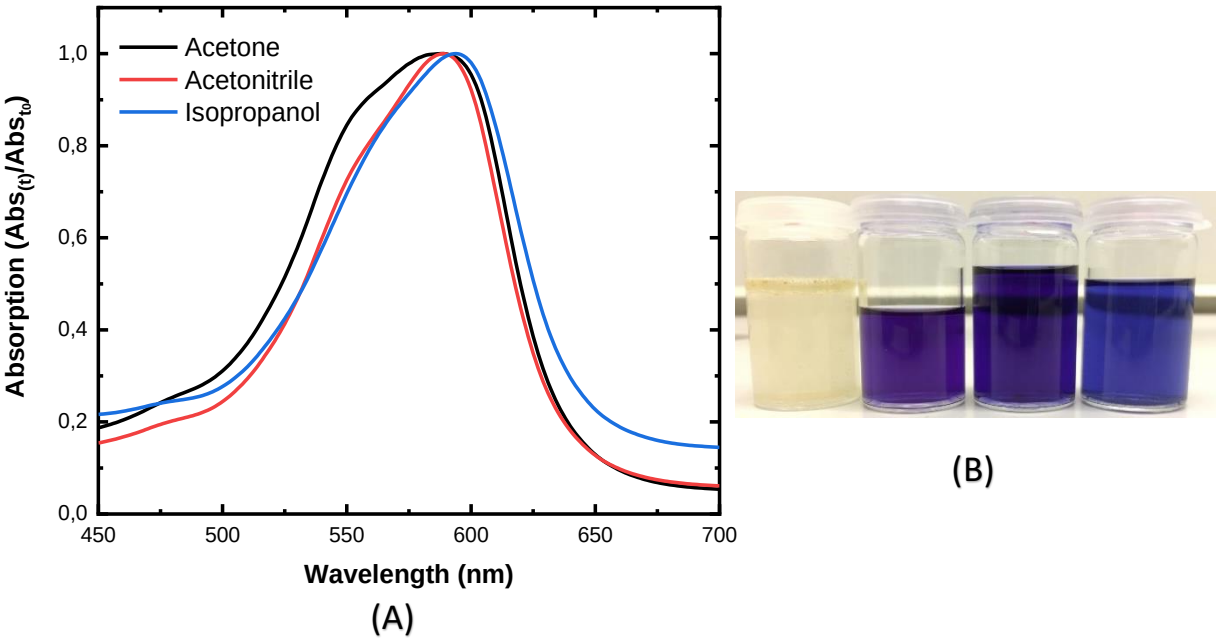

Figure 18.(A) UV-Vis absorption spectra of 2.5mM of SPO in Acetone, Acetonitrile and Isopropanol.(B) Photograph of 2.5mM of SPO in Water, Acetone, Acetonitrile and Isopropanol, respectively

SPO among many other chromic molecules can be used as detectors and sensors for many solvents as seen in absorption spectra in figure 18 (A). Where the absorption of the PMC photo-isomer is dependent on the solvent polarity, so that with increasing solvent polarity a red shift in the absorption spectrum is ensued [82]. That being said, PMC in acetone, acetonitrile and isopropanol has an absorption peaks at 588nm, 589nm, and 594nm respectively. Whereas, the photograph of figure 18 (B) shows the coloration change of SPO/PMC in multiple solvents, SPO was not dissolved in water, however it was able to dissolve in many polar and non-polar solvents such as, acetone, acetonitrile, isopropanol (shown above), toluene, benzene, DMSO and $CDCl_3$(not shown in this work). It should be noted that the coloration of the SPO is not a result on any UV exposure, but a direct coloration the occurs when the yellow powder of SPO encounters any of the aforementioned solvents.

Thus, when SPO molecules are introduced to solvents in high concentrations a thermal equilibrium between the closed SPO and the open PMC isomers within the solvent arise, whereas with increasing concentration and temperature the color deepens [82].

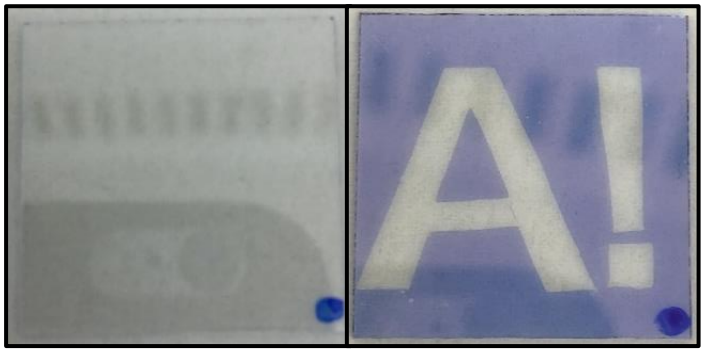

Figure 19.Photograph of a 60nm SPO film, before and after UV exposure

On the contrary, depositing SPO molecules on a substrate eliminates the need of a solvent, and probably gives a better control on the existing isomers concentrations. Since SPO is a thermo-chromic molecule, the molecule can be activated with the increase of temperature. Therefore, when evaporating SPO through thermal means then by convention all molecules that would leave the evaporation source would be in their PMC state and would later then transform to the closed state upon the condensation on the colder substrate. Subsequently, the closed SPO film can be mostly excited to their PMC isomer form by UV radiation activation as shown in figure 19.

4.1 Chemical Functionality and Thermal characteristic of SPO

Both the H1 and C13 NMR spectra, shown in figure 20, of the dissolved SPO in deuterated chloroform, where the resultant has a blue color, matches the standards supplied by Sigma Aldrich.

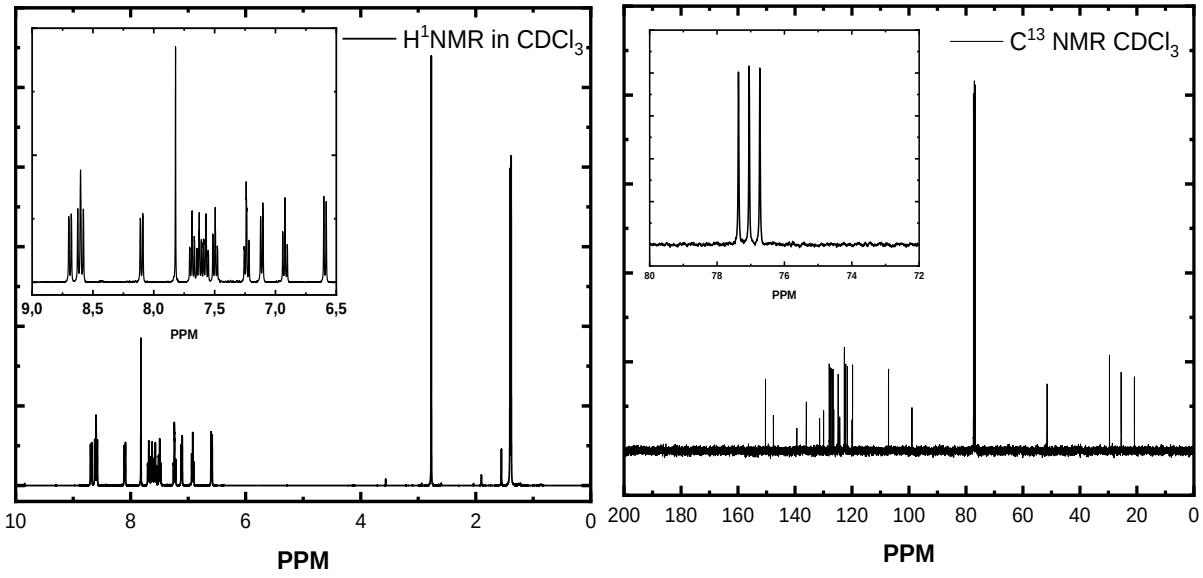

Figure 20. H1 and C13NMR spectra of SPO in deuterated chloroform.

Additionally, C13 NMR spectra of SPO has been investigated by Duck-Hyung, et al. at low temperatures, to decrease the thermal decoloration rate. Where they observed the emergence of two peaks at 172.6 ppm and 178.0 ppm when exposing the closed form SPO to UV radiation [83]. The absence of any peaks in the 170-180 ppm region in this work's C13 spectrum along with the coloration of the measured sample, furtherly indicates that a thermal equilibrium between the SPO molecules and PMC is formed.

The thermal analysis of the SPO powder was used to obtain the deposition temperature. A dip in the heat flow was observed at ~90°C, shown in figure 21, corresponds to the glass transition temperature (T_g). Most probably at this temperature the sublimation of SPO molecules commence. In addition, the steepest peak observed at ~200°C presents the melting point of the measured sample. Since the rate was relatively slow for the deposition at 90°C,

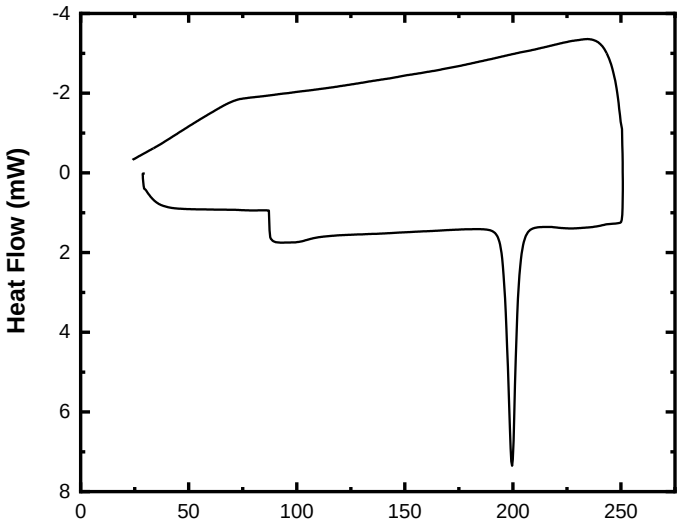

Figure 21. Thermal analysis of the powder SPO.

the deposition temperature was reassigned to 140-145°C, which resulted in a deposition rate of 1.3Å/s.

4.2 Deposited SPO Film characterization

The vacuum thermal evaporation of SPO took place at a temperature of ~140-145°C, hence the thermal energy supplied to the molecules is ~0.03 eV, which was sufficient to break the Van der Waal forces (0.01 eV) and simultaneously is still far off the range of the covalent bond (2-7 eV) [46]. However, the chemical composition of the deposited film was analyzed and compared to the powder form SPO using FTIR, as shown in the figure bellow,

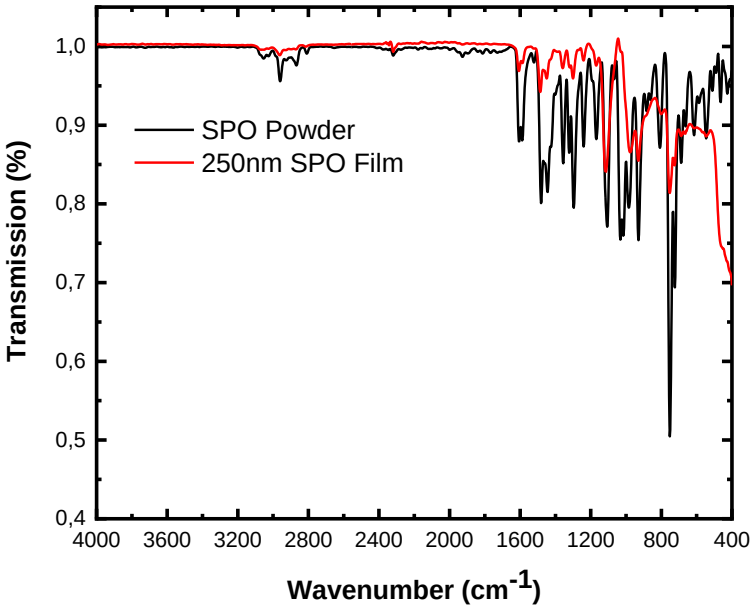

Figure 22. FTIR spectra of SPO powder, and 250nm deposited SPO film on Si wafer.

Both the powder precursor SPO and the deposited film on a silicon wafer share nearly identical FTIR spectra. However, due to the subtraction of the reference silicon wafer from the deposited sample, some of the peaks were overlapped. Peaks at 809, 985, 1010, 1295, and 1479 cm^{-1} define, the C-N bond located in the indole, while peaks at 1010 and 1350 cm^{-1} represents the C-N bonds located in the oxazine ring. Peaks at 1032, and 1108 cm^{-1} represents the C_{Spiro}-O bond, furthermore 1195 cm^{-1} characterizes the C_{Spiro}-N bond. Finally, 1605, and 1242 cm^{-1} illustrates C=N and C-O bonds, respectively [84]. Thus from the FTIR data it was determined that the deposited film actually matches the precursor material in terms of chemical integrity.

4.2.1 Surface Morphology and Substrate effects

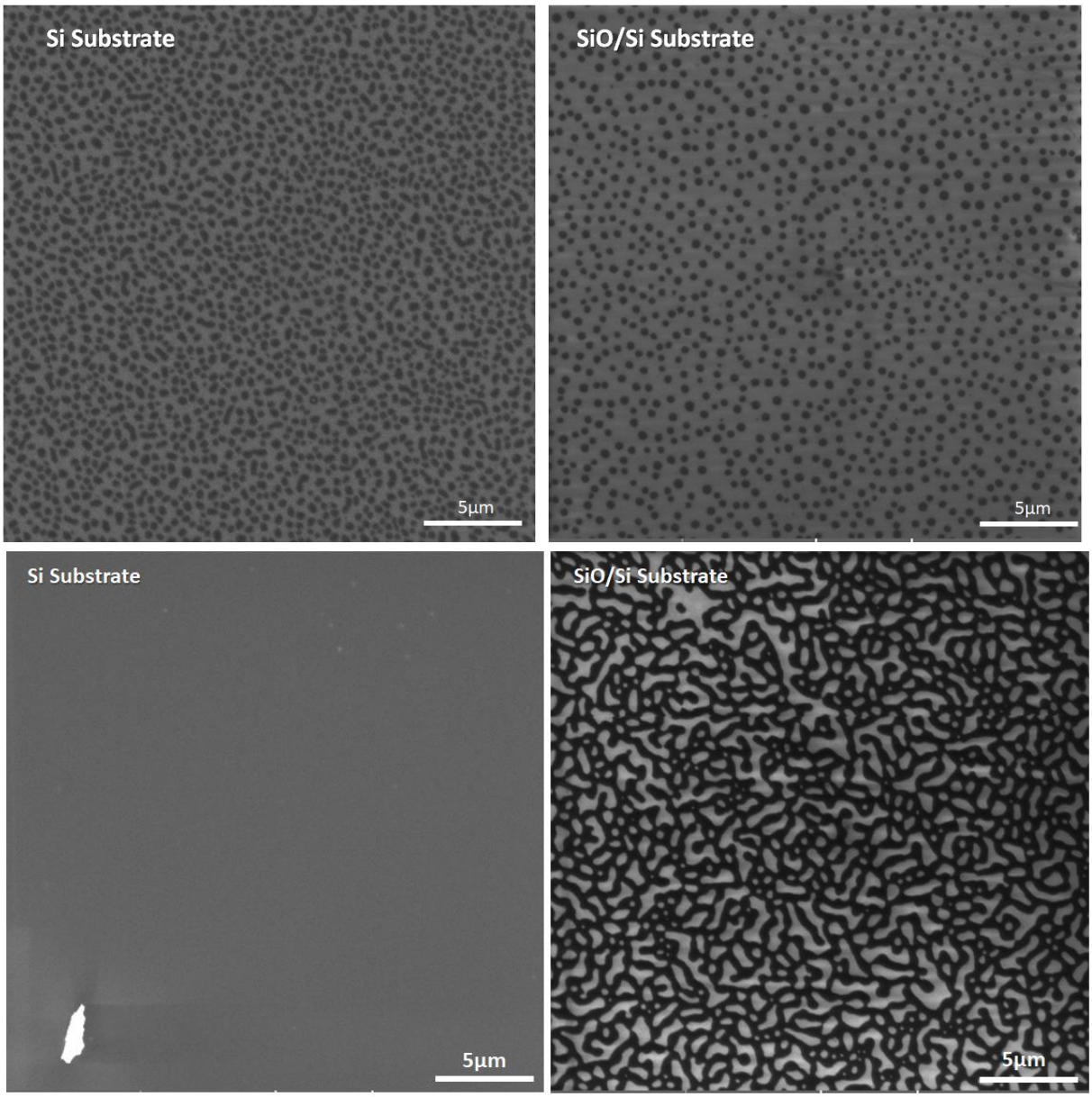

Figure 23.SEM Images for 6nm SPO thin films on both Si and SiO substrates (top), and 15nm SPO thin films on both Si and SiO substrates (bottom). All images were obtained at the same working distance and accelerating voltage.

The deposited SPO thin films were obtained at three different thicknesses. The 60nm thickness evolved a continuous film, while the 15nm resulted in percolated sample, and finally the 6nm ensued a particle sample film as shown in the SEM images in figure 23. The nucleation and growth of the SPO molecules on a substrate can be explained by Volmer-Weber mode, in which the cohesive forces between the SPO molecules are much higher than the adhesive forces between the SPO molecules and the substrate, thus these molecules will tend to aggregate and form droplets on the surface [85]. As more SPO molecules are being introduced onto the substrate in form of condensation, the distance between the particles decreases leading into percolation, where networks of SPO molecules are randomly connected. Additionally, with

further accumulation of SPO molecules, the created networks connect with each other until all the networks are connected and a continuous film is obtained. At that stage, any additional condensation of SPO molecules would result in an increase in the film thickness.

It is worth mentioning that, the cluster deposition of photochromic SPO molecules was never reported in literature is being extensively studied elsewhere by our group under the framework of ASCI project.

Besides the growth mode of the SPO thin films, it was observed that with dissimilar substrates different surface features of the deposited SPO molecules arise as shown in figure 23. When depositing 6nm of SPO molecules on both Si and SiO_x substrates, we detected that the filling factor of the SPO particles nearly doubles. In addition, when depositing 15 nm on the aforementioned substrates, it was observed that the deposition on Si substrate resulted in a continuous film, while the deposition on SiO_x substrate resulted in a percolated sample. It worth mentioning, that both the Si and SiO_x substrates were placed adjacently during the deposition process, where all conditions were similar.

The difference between the two related substrates is raised from the surface energies and the wettability of these surfaces [86, 87], which can be best explained when referring to Elbahri's expression of '*Like Wets Like*' [88]. In which the difference between the cohesive and adhesive forces that arise from the interaction of SPO molecules among themselves and their interactions with the substrate, respectively, is much lower when comparing the Si substrate to the SiO_x substrate; thus, the SPO molecules will tend to wet more the surface of the Si substrate as compared to the SiO_x surface.

4.2.2 Film Thickness

For the calibration of the QCM, a100nm (read by the QCM) SPO film was deposited on a glass substrate, where the actual thickness was measured by a profilometer. Utilizing the tooling formula displaced bellow [89] , a tooling factor of 153% was determined.

$$Tooling\ \% = 100\ x\ \frac{Actual\ Substrate\ Thickness}{Displayed\ thickness} \qquad (10)$$

The thickness of the SPO films, subsequent to the tooling adjustment were measured using an ellipsometer as shown the color contour maps in figure 24. The thickness of the SPO molecules was calculated using a Cauchy model fit on the transparent region of the film at 700 to 1000 nm, and then the full wavelength expansion fit was used by parameterizing the Cauchy model to a B-Spline model covering the entire spectrum from 200nm up to 1000nm.

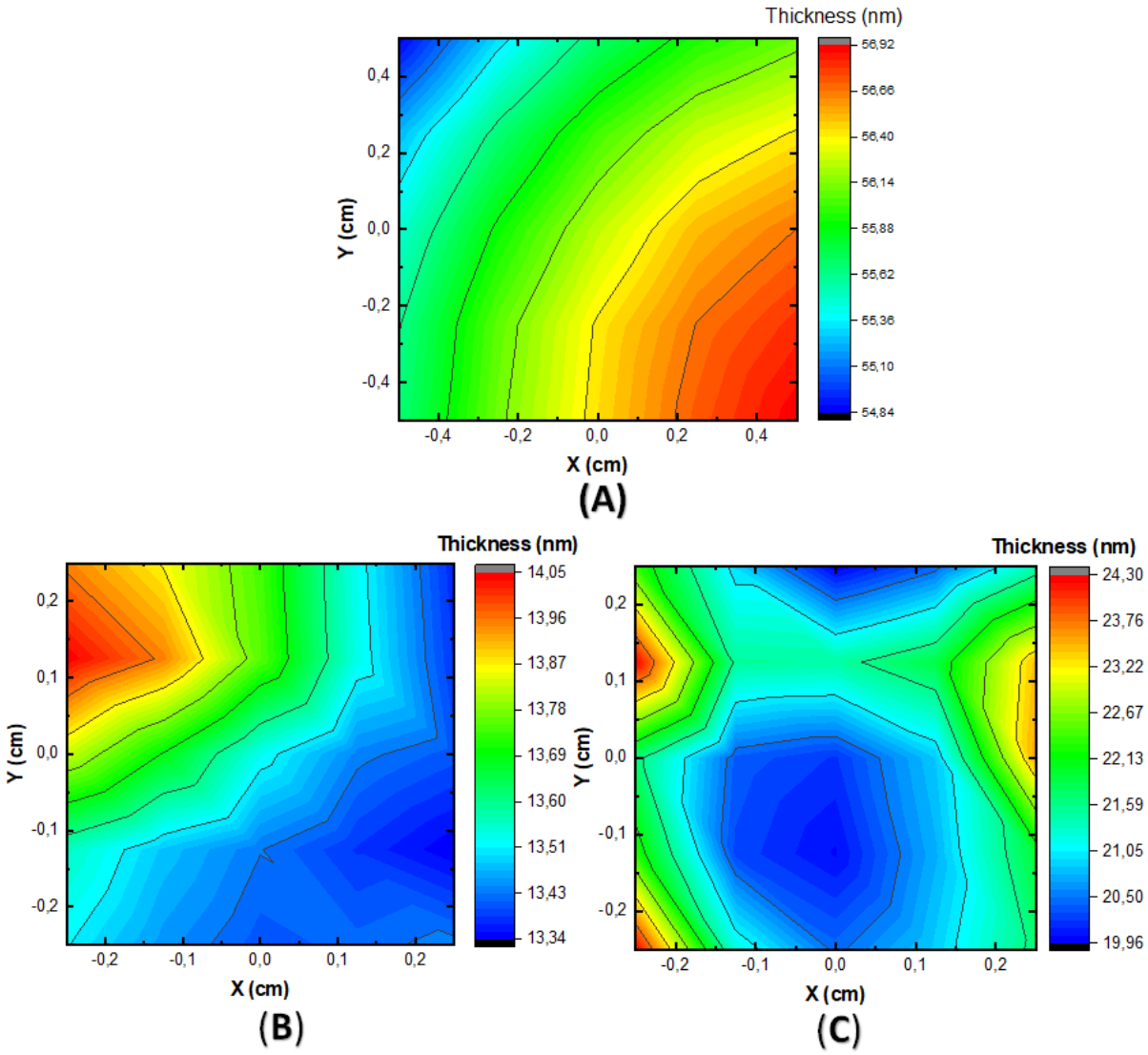

Figure 24. A contour color map of the deposited SPO films (A) 60 nm SPO thin film on SiO substrate, (B) 15nm SPO thin film of Si substrate, and (C) 15 nm SPO thin film on SiO substrate.

The deposited SPO thin film as shown in figure 24 (A) obtained a very similar thickness to the suspected thickness of 60 nm. Additionally, the radial decrease in the thickness from the left-bottom corner towards the top-right corner is a feature of the thermal evaporation profile that depends on the orifice size and the distance between the evaporator and the substrate. It should be noted that the highest thickness value is closer to the middle of the substrate holder, and as the distance from the center is increased, a variation in the thickness is observed. On the other hand, the deposited 15nm SPO thin film had two surface features depending on the substrates used. Figure 24 (B) represents the thickness map of a continuous SPO thin film as seen in Figure 23, the thickness of the film is very similar as well to the suspected thickness of 15nm and the radial decrease in thickness is still observed as it's the case with the 60nm film. On the contrary, when depositing 15nm SPO thin film on SiO_x substrate a percolated sample is

attained. Since the ellipsometer records an averaged reading for the exposed area, it was not able to detect the percolation of the SPO molecules, as shown in Figure 24 (C), neither was it able to detect and analyze the particle films using the same fitting models explained above.

Additionally, X-ray reflectivity technique was also utilized to obtain the continuous film thickness, density and surface roughness as shown in the figure 25. The obtained data was fitted using a segmented fit, which computed a film thickness of 59.457 nm, a film density of 1.08 g/cm^3, and a surface roughness of 0.565 nm. The measured thickness of the film was nearly identical to the suspected film thickness of 60 nm, whereas observed typically the measured film density is lower than the bulk density of SPO 1.2 g/cm^3. Having a lower density than bulk materials is a thin film property, which is crucial to explain the amount of porosity within the thin film [35]. Since the measured film's density is very similar to the bulk's, we conclude that the deposited film is not porous, where the molecules are stacked on top of each other closely.

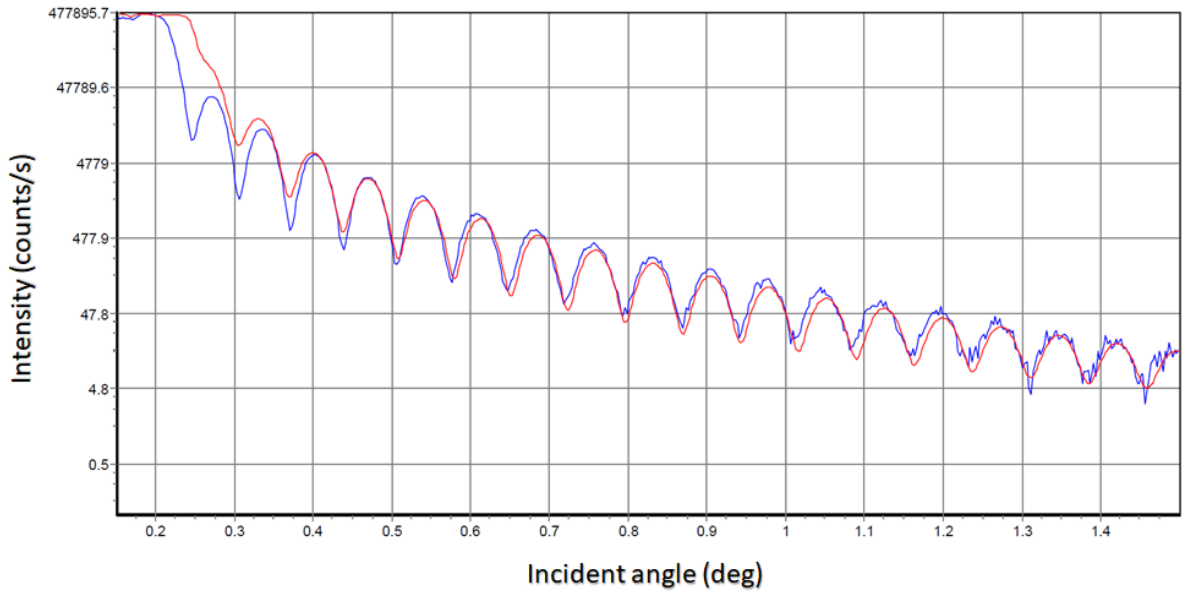

Figure 25. XRR spectrum, where the blue curves corresponds to the measured data and Red curve represents the fit.

4.2.3 Film Crystallinity

On the other hand, the deposited film crystallinity was tested via GI-XRD as shown in figure 26. The lack of any peaks signifies that the deposited film is amorphous; additionally the hump existing at 15-30° corresponds to the glass substrate amorphousness. However, few days succeeding to the deposition, we observed that the SPO films starts to crystallize.

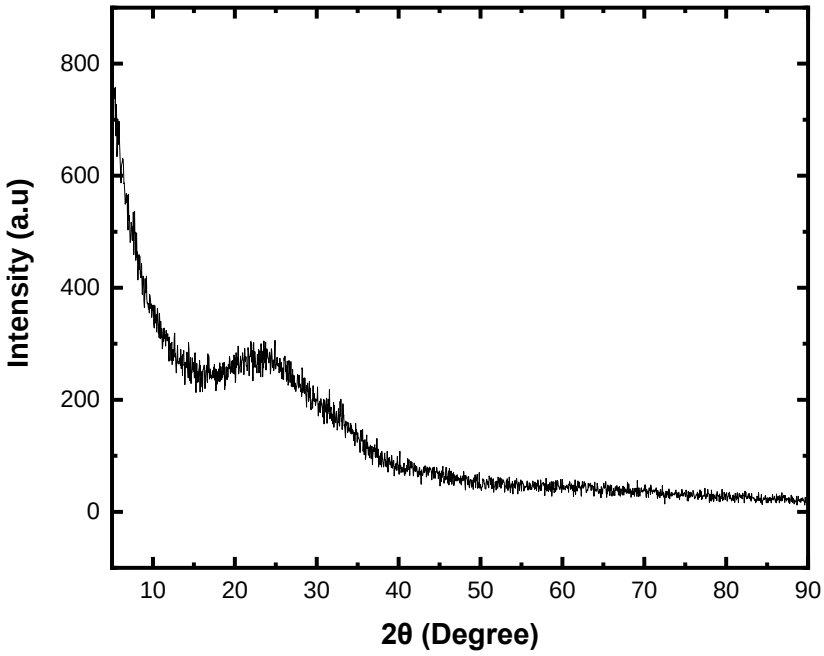

Figure 26. XRD patterns of 100nm film deposited on glass substrate.

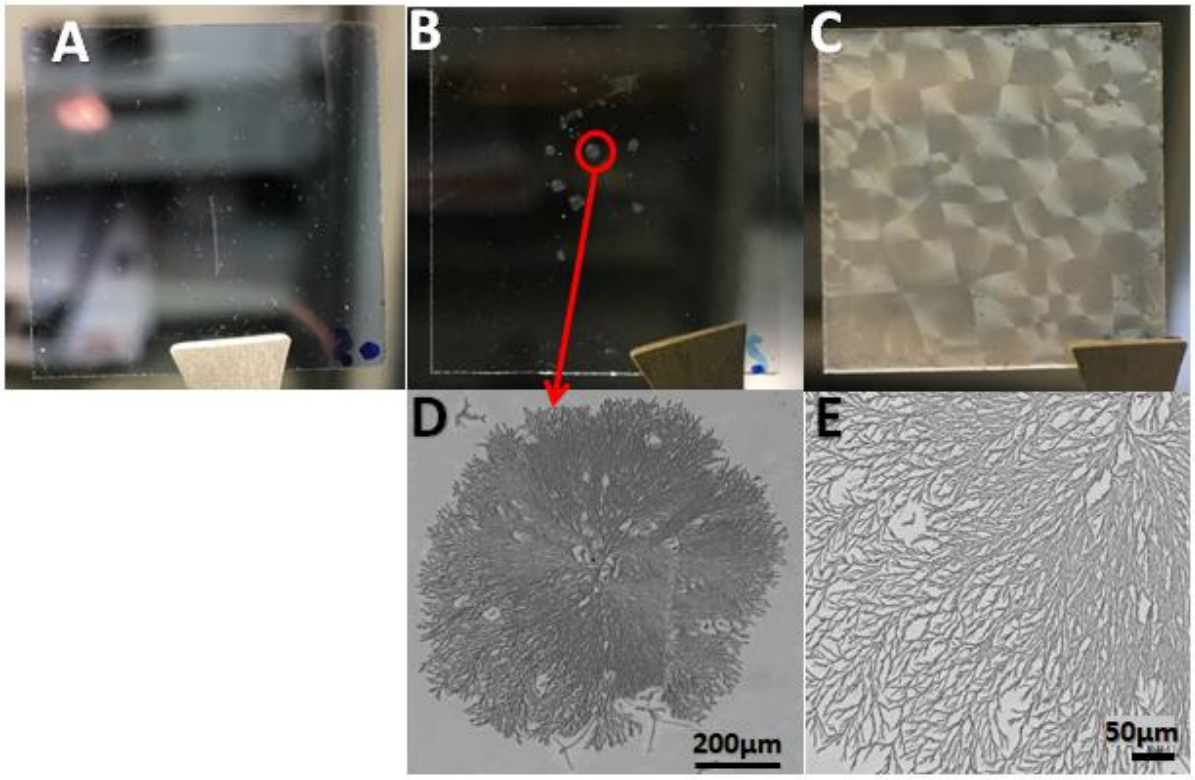

Figure 27.Optical Images of (A) 60nm SPO film, Exposed to three mins of UV radiation every 7 days (picture taken 50 days after deposition) (B) 60nm SPO film, never exposed to UV radiation (picture taken 7 days after deposition) (C) 100nm SPO film, 6 month after deposition (D) and (E)Optical microscope Images for the spherulite crystallite

Three days subsequent to the deposition, if the film was never exposed to UV radiation, it starts to crystallize, as shown in figure 27 (B). Where the formation of spherulites, can be observed with the naked eye or via an optical microscope, as it is the case in images D and E. These spherulites, containing two regions a crystalline lamella and an amorphous region, will tend to grow radially until the entire surface have been covered as it's the case in image C. The crystallization is a result of the high surface energy of the amorphous stacked SPO molecules, that generates a potential field [90]. This acts as a driving force for the surface migration of SPO molecules, which would tend to favor crystallization in order to decrease their total energy. Nevertheless, when exposing the crystallized SPO film to UV radiation, no transition towards the PMC form takes place and the film loses its photochromic ability at room temperature [82]. On the other hand, when exposing the deposited film to UV radiation, and keeping the SPO molecules in their PMC form, it was noticed that the films do not crystallize. Since the PMC is a zwitterion, a molecule that contains both a positive and negative charges [91], thus exposure to UV radiation will induce a charge separation effect within the film. Accordingly, the transformation from the closely packed SPO to the charge separated PMC would always shift the system away from crystallization.

4.3 Optical Characteristics of the Deposited SPO

When exposed to UV radiation spirophenanthrooxazine SPO molecules transforms into a semi-planer merocyanine PMC form as shown in the 3D sketch bellow.

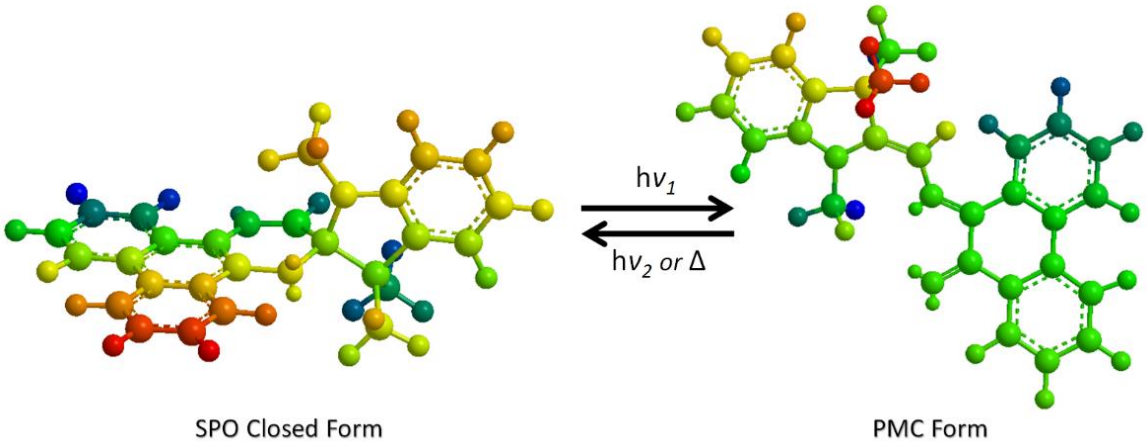

Figure 29.3D sketch of the closed SPO form and the open PMC form, whereas $h\nu_1 > h\nu_2$ and Δ represents temperature.

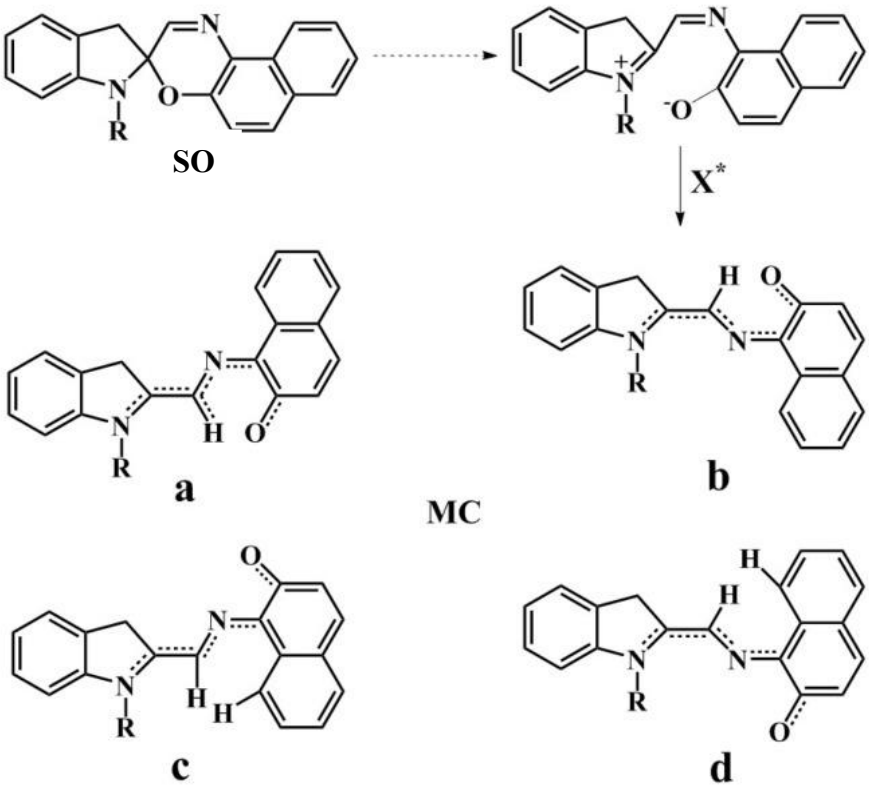

Figure 28. Chemical structure of spirooxazine, the transitional X state, and four of the most favorable MC isomer. Copyright © 2017 by [82]*

However, upon UV-radiation a transition state X^* is formed followed by rapid molecular rearrangement into more stable PMC form(s). Based on the chemical atmosphere, PMC can

co-exist in four most favorable isomers, where isomer A and B are the most thermodynamically stable isomers due to conformational steric barriers [82] ,as shown in figure 29.

The optical properties including transmission, reflection and absorption of the deposited SPO film with different features were obtain via a UV-Vis spectrometer equipped with integrated sphere sample stage. Multiple cycles of UV radiation were exposed to the desired sample before the measurement. The cycle term is used to express an exposure of 2 minutes of white light followed by 3 minutes of UV radiation in the case of continuous films, while for percolated and particle samples the white light and the UV radiation exposure were 1 and 2 minutes, respectively.

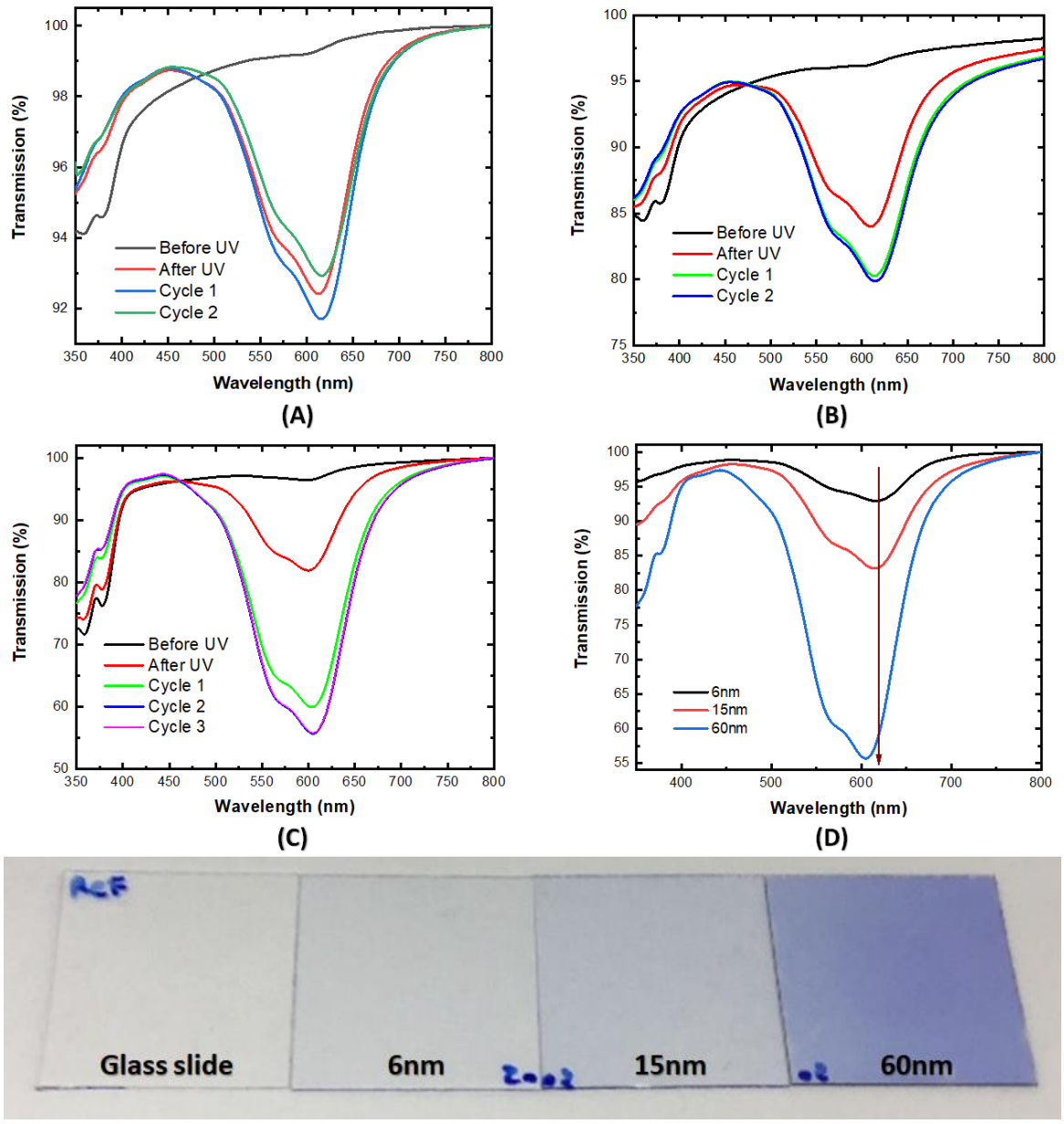

Figure 30.UV-Vis Transmission spectra of (A) 6nm SPO, (B) 15nm SPO and (C) 60 nm SPO on glass substrates (D) minimum transmission of all films. Bottom: image of the deposited films at minimum transmission.

In the figure above, the transmission spectra of the deposited films were obtained at multiple cycles until a maximum absorption/minimum transmission was obtained. As presented, with increasing film thickness from 6nm particle to 15 nm percolated and until finally a 60 nm continuous film more cycles are needed to achieve the maximum absorption/ minimum transmission point. This phenomenon occur due the high film density, the packed stacking and restricted rotation of the SPO molecules. When exposed to the first 3 minutes of UV radiation, most of the SPO molecules will transform instantaneously into the zwitterionic merocyanine intermediate, however some SPO molecules will tend not to transforms due to the confinement constrains. Yet with repeated cycles, the SPO molecules will be readily more accessible to the stimuli (UV-light), where all their dipole moments are triggered, figure 31.

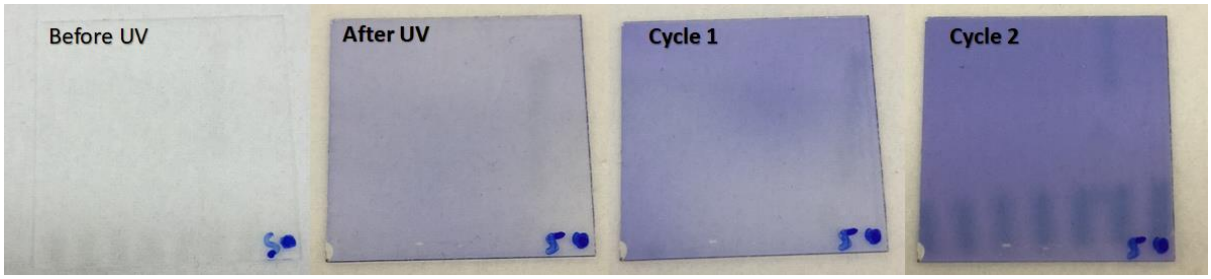

Figure 31.Images of 60nm SPO film, before UV, After UV, after Cycle 1 and finally after cycle 2.

The dip in the transmission spectra of SPO, figure 30, before UV exposure at ~375nm occurs due to the excitation of an electron from a π-bonding level to a π^*-antibonding level in a process known as $\pi - \pi^*$ transition [92]. While the broad dip in the transmission peak after the UV illumination at 615nm originates from the n- π^* transition, and it is a resultant of both the photo-isomer A and B, in Figure 28; which absorption peaks are 599nm and 605nm, respectively. Additionally, the shoulder peak located at ~567 nm is due to photo-isomer C that has the largest dipole moment [82].

Figure 30 (D) shows the minimum transmission of all the films produced in this work, where a clear blue shift is observed with increasing film thickness. Thus, with increasing film thickness, the lower the free volume of the system is and more energy is required to push the system from a relaxed stable mode towards the excited colored mode.

The specular reflectivity of the SPO molecules before and after UV radiation were obtained at an angle of eight degrees as shown in the figures bellow.

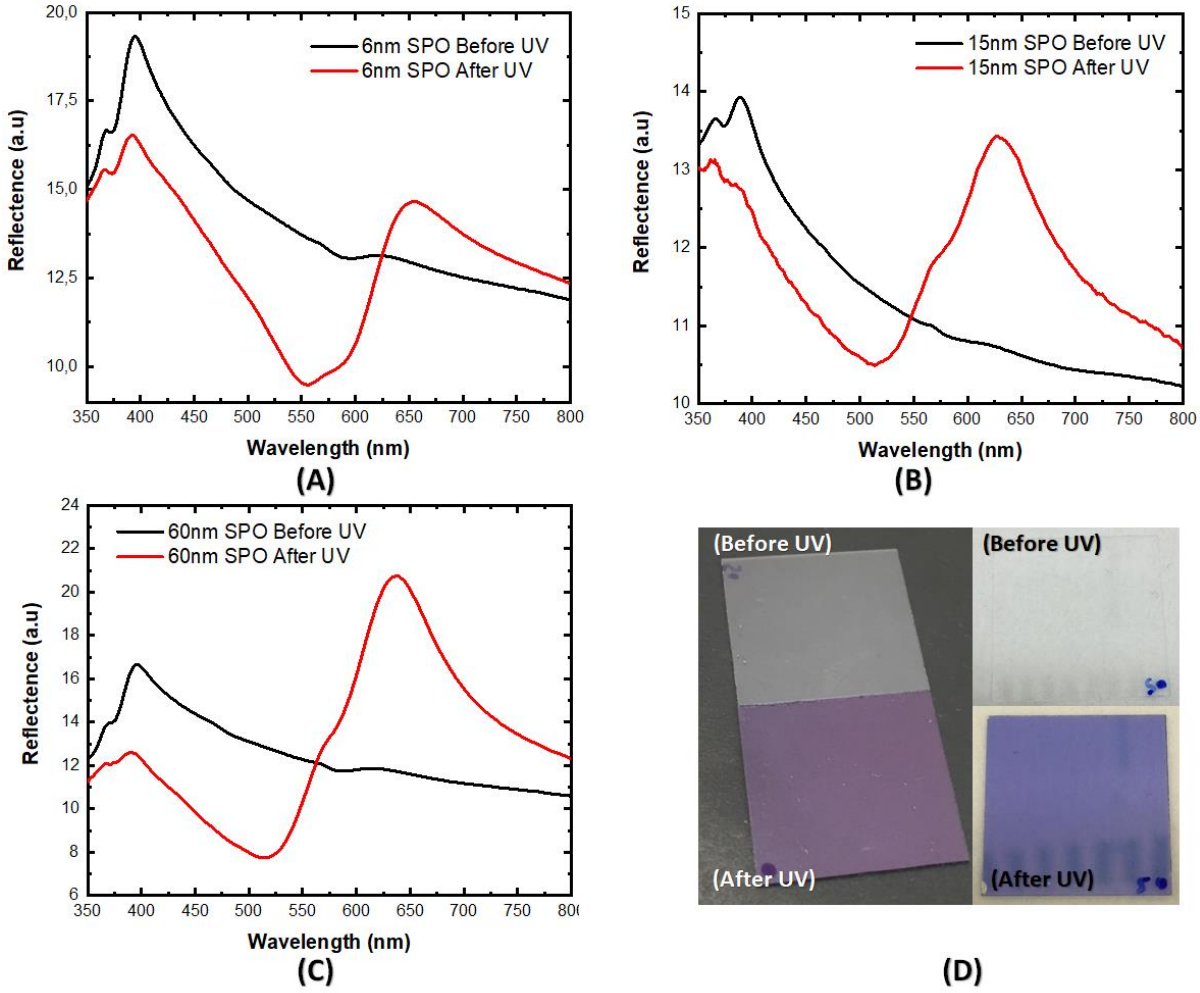

Figure 32.Specular Reflectance spectra of (A) 6nm SPO thin film, (B) 15nm SPO thin film, (C) 60 nm SPO thin Film and (D) photographic images of 60nm SPO films before and after UV on both a black and white background.

The blueish color of the PMC films, figure 19, originates from the electronic n- π^* transition, figure 30. Yet, our group has also showed recently that these molecules are capable of reflecting light at their resonance frequency, figure 32 (A-B-C), in a phenomenon known as polarizonic [93, 94]. Thus, PMC films are able to exhibit two colors at the same frequency [40], figure 32 (D).

4.4 Thermal-, and Solvato-bleaching

In this section we are opted to explore the decay dynamics of the SPO/PMC thin films with and without the influence of exposure to VOCs. It is worthy mentioning that the cluster based SPO are not presented here due to the detection limit limitation of the CCD camera based detector mounted in the fiber optic spectrophotometer.

The room temperature inherent decay dynamics of the PMC film into bleached SPO form has been recorded for both the percolated sample and the continuous films as shown in the figure bellow.

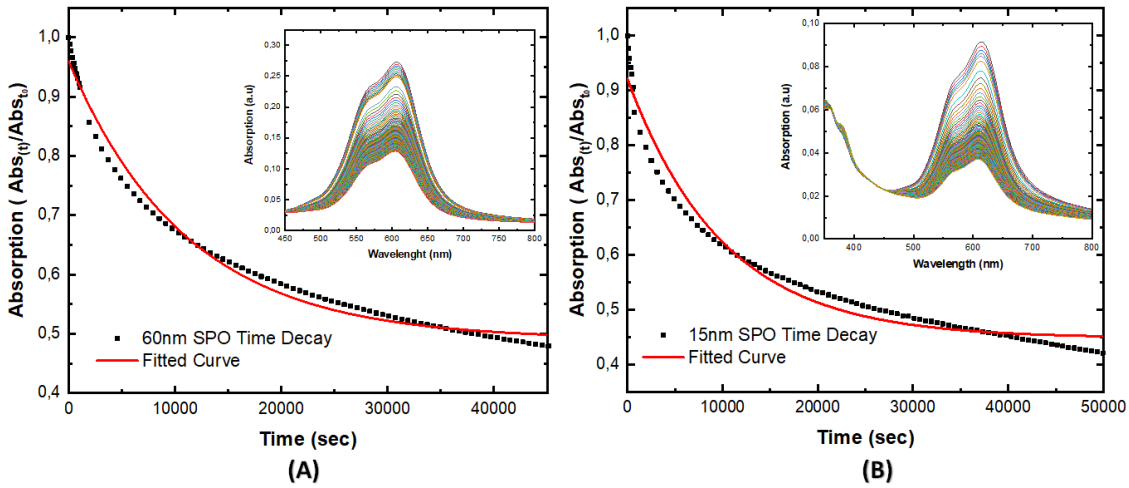

Figure 33. Time-resolved Absorption Spectra at 600nm for (A) 60 nm SPO continuous film and (B) 15nm SPO percolated film, whereas the embedded figures show the original data.

The absorption peak maxima located at 600 nm was monitored chronologically, where the collected data was fitted with a model based on a first order decay equation shown below (equation 11). Inspection of the fitting parameters was done to obtain the thermal bleaching rate constant (k) of the decay occurring at room temperature [95].

$$A(t) = A_{min} + A_o e^{-kt} \qquad (11)$$

The rate constant of both the 60 nm and 15 nm samples was k = 8.99×10^{-5} s^{-1} and 9.94×10^{-5} s^{-1} with a half-life time ($t_{1/2}$) values of 7708,5 and 6971,8 seconds , respectively.

On the other hand, when exposing the PMC samples to multiple volatile organic compounds, a dramatic acceleration in the decay was observed, in which the bleaching time was reduced from 13 hours down to few seconds. To the best of our knowledge such phenomenon has not been recorded or presented in literature, so a new term is introduced, solvato-bleaching, which describes the color discharge of the photochromic thin films through the exposure of chemical vapors.

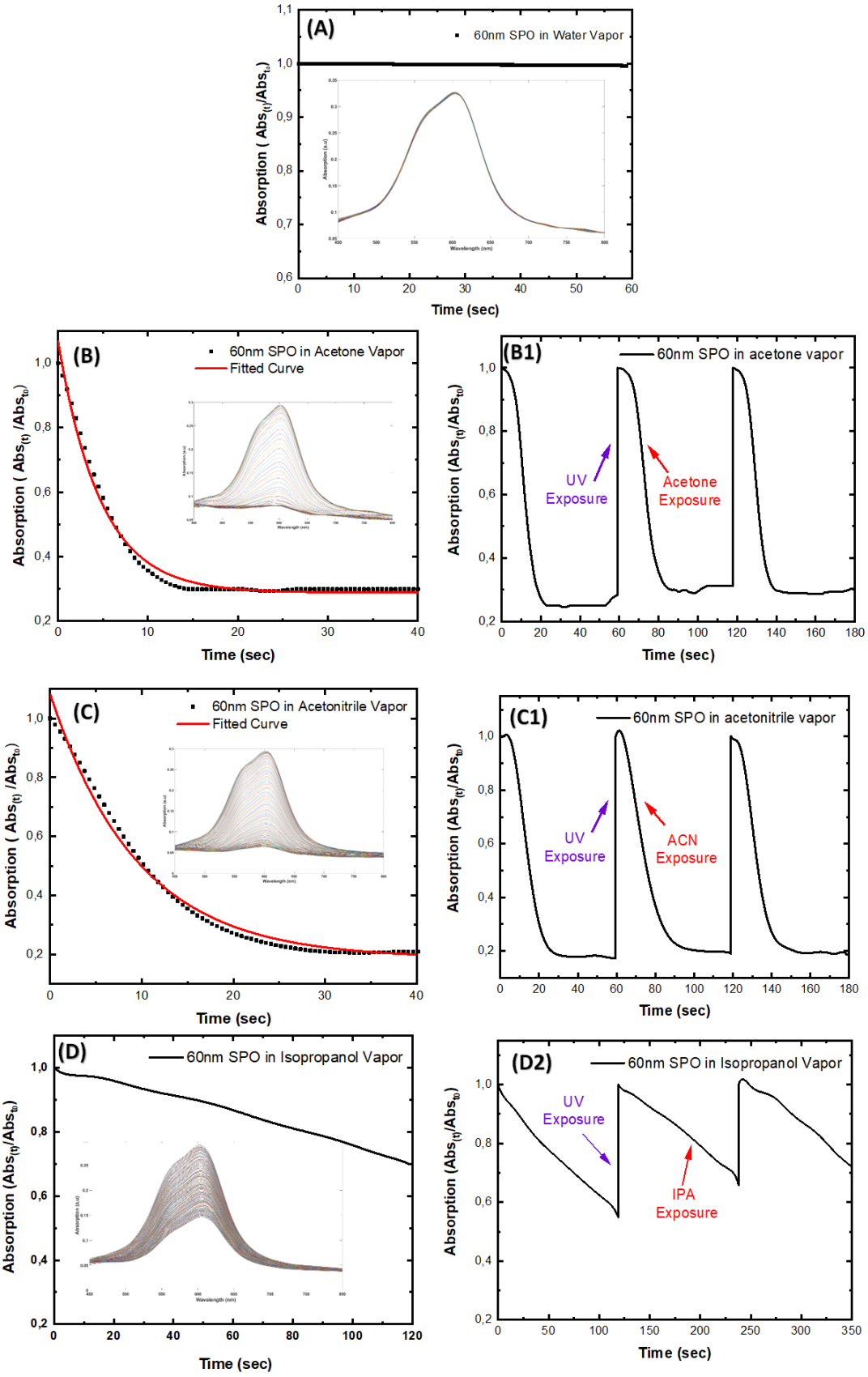

Figure 34. Time-resolved absorption spectra at 600nm of 60 nm SPO thin film where it was exposed to (A) Water Vapor (B) Acetone vapor (C) Acetonitrile vapor, and (D) Isopropanol Vapor, whereas the embedded figure show the original data. The figures denoted as (B1), (C1) and (D1) show the cyclability of these thin films.

As shown in the figure 34 (A), exposing the colored PMC film to water vapor results in no action and the film remains intact. This result indicate that the SPO/PMC film is water vapor resistant. This inherent surface feature of the deposited SPO/PMC film would be very beneficial if the film was considered to become an industrial product, where humidity degradation is one of the main failure that thin films encounter [96]. On the other hand, Figure 34 (B) reveals the response of the PMC film upon exposure to acetone, in which the film decays 70% of its absorption in just 10 seconds. In addition, according to the fitting model used the acetone driven bleaching is 0.217±0.014 s^{-1}. Correspondingly, placing a PMC film in acetonitrile vapor exhibit a similar behavior to acetone; yet, a slower color-fading rate with a value 0.130±0.019 s^{-1} was observed. Finally, due to device limitation and the intrinsically low vapor pressure of isopropanol (IPA), an expected exponential decay under the influence of IPA was not achievable under the constrains of the isolated gas phase chamber which was designed to eliminate any matrix effect. However, in order to exclude the instrumentation barriers figure 35 shows the ability of the isopropanol to induce an exponential decay the 60 nm film under atmospheric pressure, where the time in figure (B) resembles the total exposure time to highly concentrated isopropanol vapor. According to the obtained data, the longer time needed for isopropanol to decay implies the lower bleaching rate compared to its acetone and acetonitrile analogous vapors.

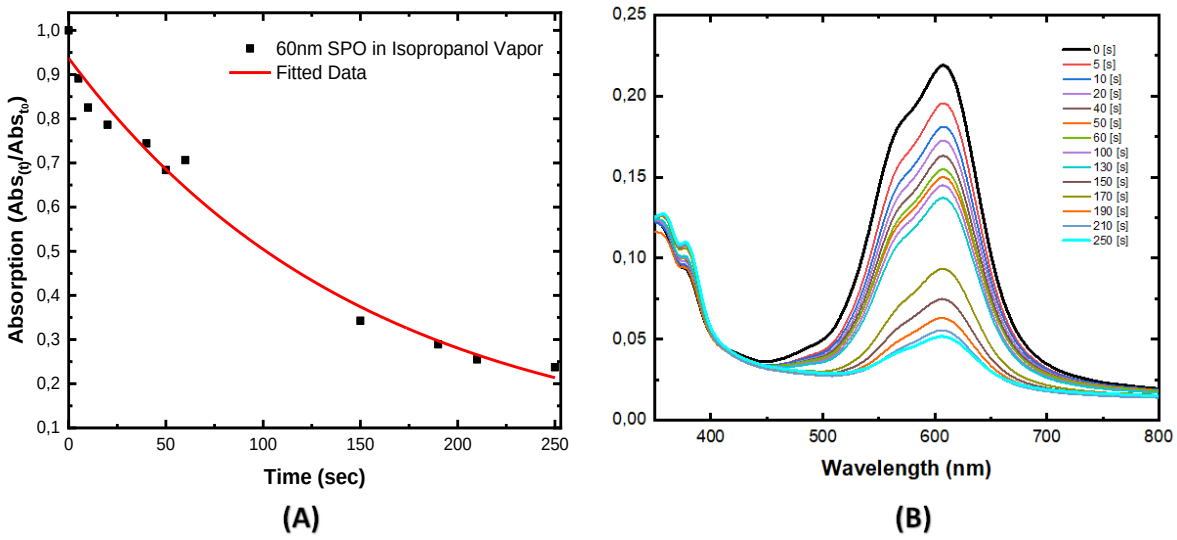

Figure 35. Time-Resolved absorption of 60nm SPO film using Isopropanol vapor (A) at 600nm and (B) original data.

In order to stand on the nature of the decay process whether it is kinetic, adsorption or mixed controlled an extra experiment was proposed as following; exposing a PMC film to a short pulse (2 seconds) of one of the aforementioned vapors, and observing its decay dynamics

profile as shown in the figure 36. It was concluded that the rate determining step of the decay process is kinetically (diffusion) controlled with no or very limited adsorption barrier. Such conclusion was based on the fact that if the decay process is a adsorption limited process the film a sigmoidal profile will persist.

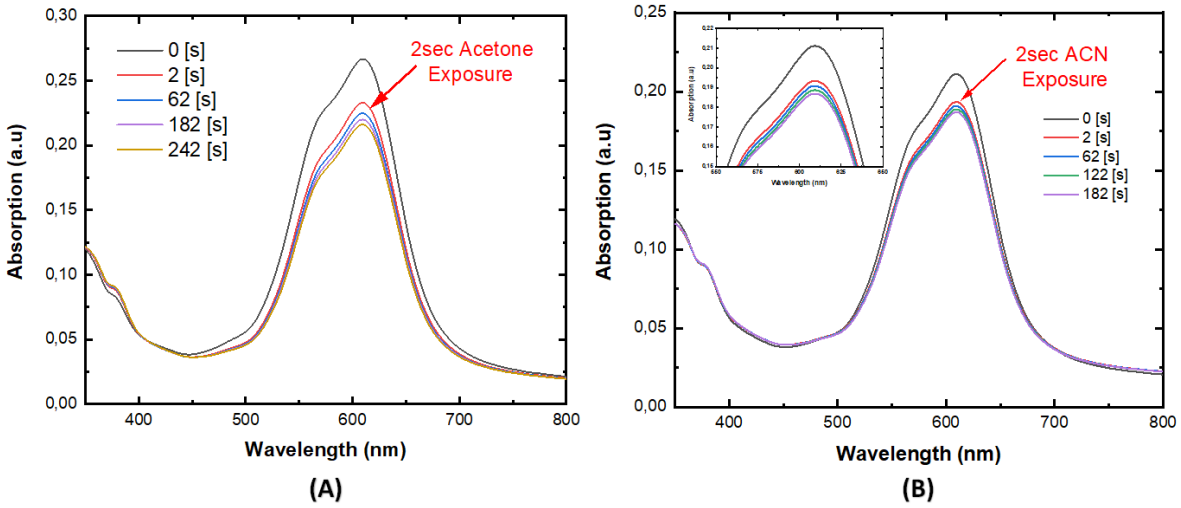

Figure 36. Time-resolved absorption of 60nm SPO thin film, before and after the exposure of a single 2-second pulse of both (A) Acetone and (B) Acetonitrile vapors.

The solvatobleaching process is resulted from the interactions between the solvent vapor and the PMC film. The rate of PMC conversion into SPO is highly dependent in many chemical and physical features of the VOC including concentration, dielectric properties, and steric conformation. A proposed mechanism for such interaction was formulated as follows; it is well established in literature that the PMC form hold a higher dipole moment compared to its SPO counterpart [82]. Hence, resembling the role of thumb concept '*like dissolves like'* the relative stability PMC/SPO films is highly dependent on the polarity matching/mismatching with surrounding medium (vapor). In this context, the lower the polarity of the vapor the lower the stability of the PMC form and the faster the decay rate and vice versa. The observed apparent decay rates were collected and summarized in table 4.

Organic Compound	Solvent Polarity Index (E_T^N)	Solvato-bleaching rate (s^{-1})
Water	1	0
Isopropanol	0.617	0.0018*
Acetonitrile	0.460	0.130±0.019
Acetone	0.355	0.217±0.014

*Table 4. The relationship between the solvent polarity, obtained from [97], and the solvato-bleaching rate. *The solvato-bleaching rate is a preliminary result, and it is used as a proof of concept.*

According to the results given in figure 37, the percolated SPO/PMC film was found to be faster that it continuous film analogous as expected due to the relatively higher surface energy of the surface. However, surprisingly the response pattern of the percolated sample was showing a twist to our abovementioned proposed mechanism. The dependency of the stability of the PMC/SPO forms with the corresponding surrounding vapor polarity is no longer preserved where ACN vapor was giving a faster decay rate compared to acetone.

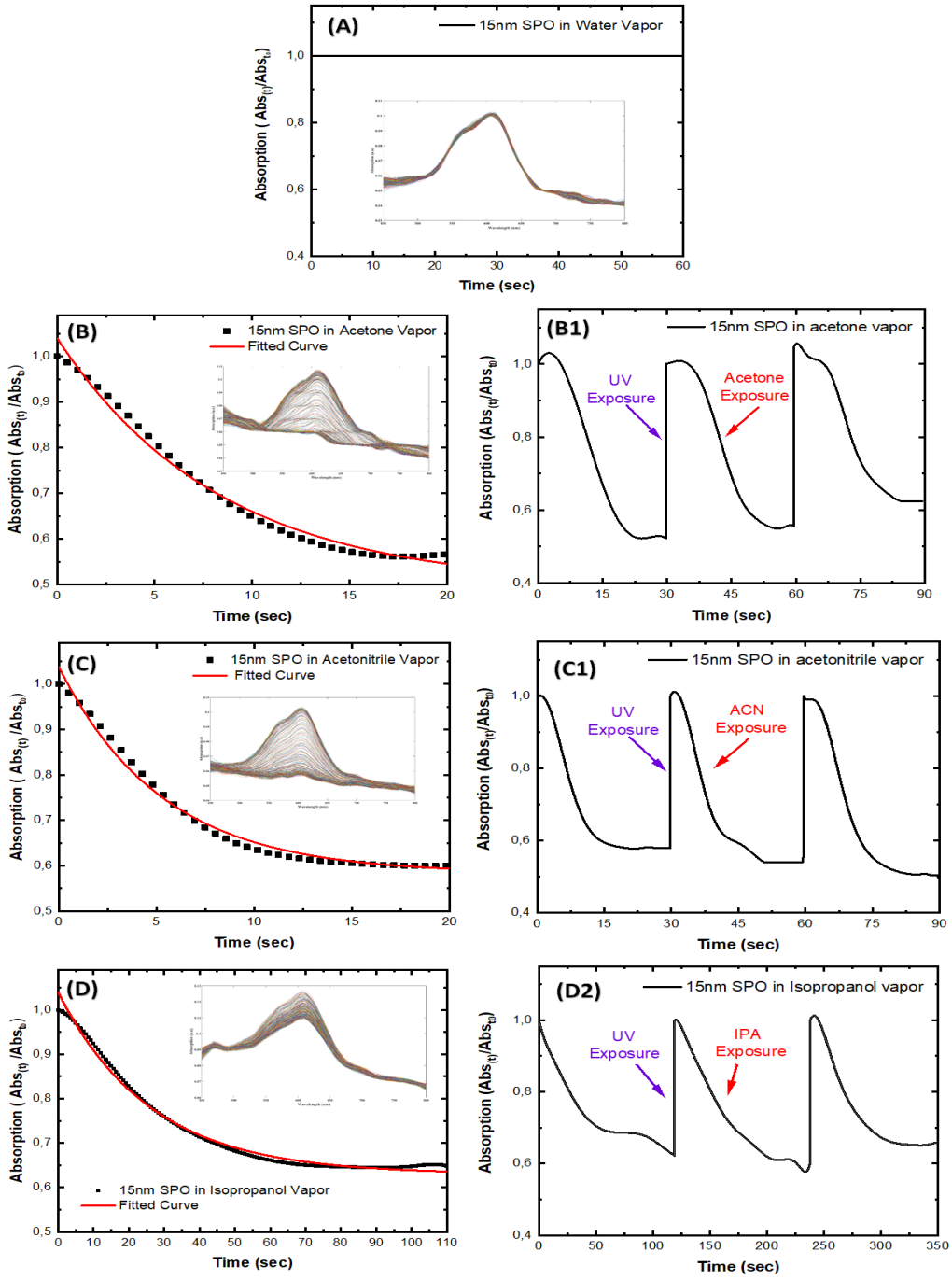

Figure 37. Time-resolved absorption spectra at 600nm of 60 nm SPO thin film where it was exposed to (A) Water Vapor (B) Acetone vapor (C) Acetonitrile vapor, and (D) Isopropanol Vapor, whereas the embedded figure show the original data. The figures denoted as (B1), (C1) and (D1) show the cyclability of these thin films.

Furthermore, because of provoked kinetics, IPA was behaving ideally with an expected exponential decay. The rates of solvato-bleaching for Acetone, Acetonitrile and Isopropanol are 0.139 s^{-1} ± 0.007, 0.199 s^{-1} ± 0.030, and 0.0316 s^{-1} ± 0.006, respectively.

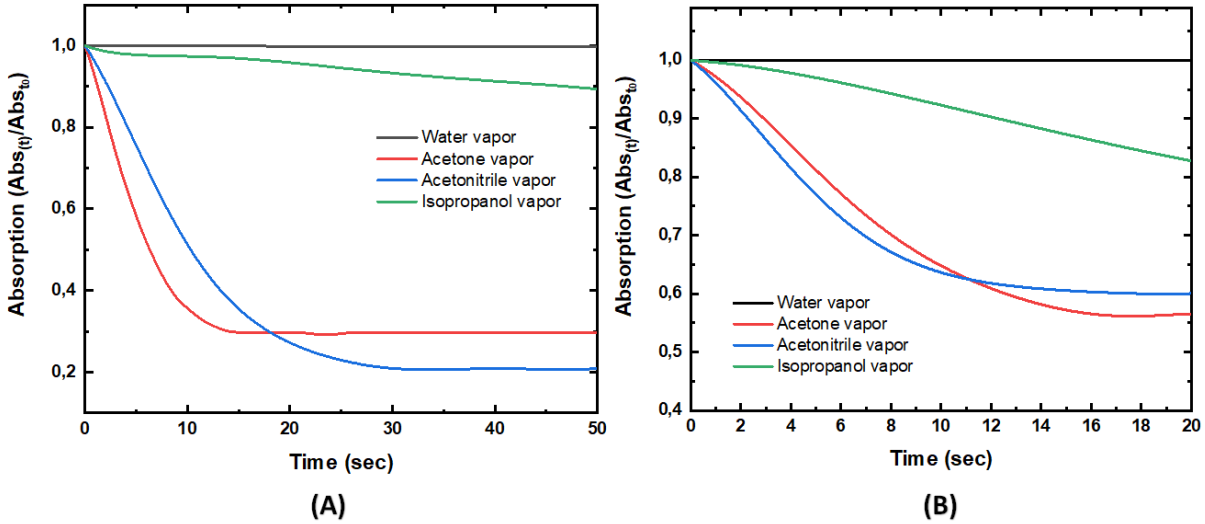

Figure 38. Time-resolved absorption at 600nm of (A) 60nm and (B)15nm SPO film under the influence of multiple vapors.

The clear flip over observed in the decay profiles under the influence of ACN and acetone vapors can be explained through taking the steric configuration of the vapors connected to the vicinity of the PMC/SPO interface. The percolated sample tend to form a more curved surface compared to a flat surface in case of continuous film. The vapor molecules striking a curved surface and adsorb will be more sterically hindered compared to the planner surface (continuous film) as given in the illustrative schematics figure 39. Because of the existence of two bulky methyl groups in Acetone compared to linear dipolar ACN, the excess surface concentration in acetone will be strictly limited compared to ACN. In addition, the relative surface concentration is not the solely factor causing such twist in the decay profile. The geometry factor will play an extensive role in defining the strength of dipolar interactions between the vapor molecules and the surface.

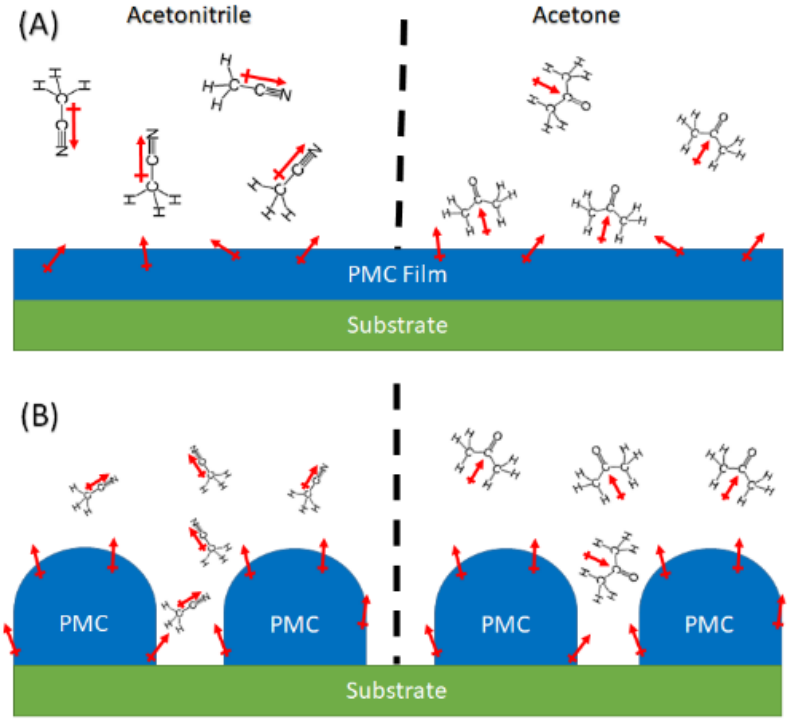

Figure 39. Cross section graphical illustration of the interactions between the solvent molecules and the PMC where the red arrows (A) continuous film and (B) percolated sample.

5 Conclusion & Outlook

In conclusion, the deposition of multiple thicknesses standalone Spirophenanthroxazine molecules on various substrates was executed through the means of evaporative deposition. The deposited films were studied for their chemical integrity, thickness, crystallinity, surface morphology, density, and photochromic ability. In addition, the interactions between the films and the organic compound vapors were examined in a state-of-the-art gas-phase chamber. From the obtained results a new and an unreported term, Solvato-bleaching, was set to describe the decay kinetics of the colored photo merocyanine isomer when exposed to chemical vapors. Where it was concluded that the solvent polarity determines the rate of solvato-bleaching in continuous film, yet some exceptions may take place when the surface morphology changes (e.g. from a flat surface ‘continuous film’ to a semi-cylinder ‘percolated sample’). Thus, a rise of a surface limited interaction occurs due to the geometry of the solvent, and the dipole moments of the colored photo merocyanine isomer and the solvent. Finally yet importantly, it was also observed that the deposited amorphous film tend to crystallize in a few days subsequent to the deposition, due to the high potential energy, wherein the crystalline phase poses no photochromic activity at room temperature. However, exposing the SPO film to UV radiation will promote a charge separation between the PMC molecules that would hinder the crystallization, as long as the film is in its colored form.

As an outlook for this thesis, a mathematical model could be achieved, which predicts the polarity of the exposed solvent based on its photochemical decay rate constant. Additionally, the embedment of plasmonic silver nanoparticles (NPs) within the SPO matrix could be studied, thus observing the effect of plasmonic/electronic transition coupling phenomenon occurring between the NPs and the SPO matrix on the selectivity and sensitivity of the sensor. Lastly, the polarizonic effect could be deployed as a new route towards more visualized detector based on naked eye recognition, which relies on the specular reflection rather than the absorption spectra.

6 References

[1] C. M. Lieber, "One-dimensional nanostructures: chemistry, physics & applications," *Solid state communications,* vol. 107, no. 11, pp. 607-616, 1998.

[2] R. Yu, Q. Lin, S.-F. Leung and Z. Fan, "Nanomaterials and nanostructures for efficient light absorption and photovoltaics," *Nano Energy,* vol. 1, no. 1, pp. 57-72, 2012.

[3] H.-Q. Yin, M.-X. Jia, S. Yang, P.-P. Jing, R. Wang and J.-G. Zhang, "Development of a highly sensitive gold nanoparticle probe-based assay for bluetongue virus detection," *Journal of Virological Methods,* vol. 183, no. 1, pp. 45-48, 2012.

[4] H. Kung and M. Kung, "Nanotechnology: Applications and potentials for heterogeneous catalysis," *Catalysis Today,* vol. 97, no. 4, pp. 219-224, 2004.

[5] C.-T. Wang, Lai, D.-L. and M.-T. Chen, "Synthesis of iron-doped vanadium-tin oxide nanocrystallites for CO gas sensing," *Materials Letters,* vol. 64, no. 1, pp. 65-67, 2010.

[6] W. D. Nix, "Mechanical properties of thin films," *Metallurgical transactions A,* vol. 20, no. 11, p. 2217, 1989.

[7] A. Z. Moshfegh, H. v. Känel, S. C. Kashyap and M. Wuttig, Physics and Technology of Thin Films, World Scientific, 2003.

[8] V. Schneider, O. Polonskyi, T. Strunskus, M. Elbahri and F. Faupel, "Light-induced Conductance Switching in Photomechanically Active Carbon Nanotube-Polymer Composites," *Scientific reports,* vol. 7, no. 1, p. 9648, 2017.

[9] M.-M. Russew and S. Hecht, "Photoswitches: From Molecules to Materials," *Advanced Materials,* vol. 22, pp. 3348-3360, 2010.

[10] P. M. Martin, Handbook of deposition technologies for films and coatings: science, applications and technology, William Andrew, 2009.

[11] J. R. Creighton and P. Ho., "Introduction to chemical vapor deposition (CVD)," in *Chemical vapor deposition 2,* vol. 2, 2001, pp. 1-22.

[12] R. S. Pessoa, M. A. Fraga, C. W. and H. S. Maciel, "Exploring the Properties and Fuel Cell Applications of Ultrathin Atomic Layer Deposited Metal Oxide Films," in *Emerging Materials for Energy Conversion and Storage*, Elsevier, 2018, pp. 83-114.

[13] C. Bishop, Vacuum deposition onto webs, films and foils, William Andrew, 2011.

[14] R. W. Johnson, A. Hultqvist and S. F. Bent, "A brief review of atomic layer deposition: from fundamentals to applications," *Materials today,* vol. 17, no. 5, pp. 236-246, 2014.

[15] M. Ritala, M. Leskelä, E. Nykänen, P. Soininen and L. Niinistö, "Growth of titanium dioxide thin films by atomic layer epitaxy," *Thin Solid Films,* vol. 225, no. 1-2, pp. 288-295, 1993.

[16] R. Morent and N. De Geyter, " Improved textile functionality through surface modifications," in *Functional Textiles for Improved Performance, Protection and Health*, Woodhead Publishing, 2011, pp. 3-26.

[17] K. S. Harsha, Principles of Vapor Deposition of Thin Films, CA, USA: ELSEVIER, 2006.

[18] K. Seshan, "Sputter Processing," in *Handbook of Thin Film Deposition - Techniques, Processes, and Technologies (3rd Edition)*, Elsevier, 2012, pp. 56-73.

[19] P. Bhattacharya, R. Fornari and H. Kamimura, Comprehensive Semiconductor Science and Technology, Newnes, 2011.

[20] M. M. Hassan, "Preparation and Antibacterial Properties of Reactive Surface Coatings Using Solar Energy Driven Photocatalyst," in *Handbook of Antimicrobial Coatings*, Elsevier, 2018, pp. 89-107.

[21] H. Adachi, T. Hata and K. Wasa, "Basic Process of Sputtering Deposition," in *Handbook of Sputtering Technology (Second Edition)*, William Andrew, 2012, pp. 295-359.

[22] Q. Wei, Y. Xu and Y. Wang, "Textile surface functionalization by physical vapor deposition (PVD)," in *Surface Modification of Textiles*, Woodhead Publishing, 2009, pp. 58-90.

[23] M. Ohring, Materials Science of Thin Films, New Jersey: Elsevier, 2002.

[24] D. M. Mattox, "Vacuum Evaporation and Vacuum Deposition," in *Handbook of Physical Vapor Deposition (PVD) Processing (Second Edition)*, William Andrew, 2010, pp. 195-235.

[25] M. Silberberg, A. (2006). Chemistry (4th ed.). pp. . ISBN 0-07-296439-1., New York: McGrew-Hill, 2006.

[26] H. DeVoe, Thermodynamics and Chemistry, Maryland: Prentice-Hall, 2001.

[27] S. Devender, D. Balraj and K. V. Satish, Comprehensive Engineering Chemistry, New Delhi: I.K International Publishing House, 2008.

[28] L. I. Maissel and R. Glang, Handbook of Thin Film Technology, New York: McGraw-Hill, 1970.

[29] M. Knudsen, *Annalen der Physik*, vol. 47, p. 697, 1915.

[30] H. Hertz, *Annalen der Physik*, vol. 17, p. 177, 1882.

[31] T. Young, "III. An essay on the cohesion of fluids," *Philosophical transactions of the royal society of London*, vol. 95, pp. 65-87, 1805.

[32] H. Föll, "Nuclation in General," [Online]. Available: https://www.tf.uni-kiel.de/matwis/amat/semitech_en/kap_3/backbone/r3_3_2.html. [Accessed 25 March 2019].

[33] X.Liang, D.M.King and A.W.Weimer, "Ceramic ultra-thin coatings using atomic layer deposition," in *Ceramic Nanocomposites*, Woodhead Publishing, 2013, pp. 257-283.

[34] M. Ohring, "Why are thin films different from the bulk?," *Laser-Induced Damage in Optical Materials*, vol. 2114, pp. 624-639, 1993.

[35] S. Franssila, Introduction to microfabrication, John Wiley & Sons, 2010.

[36] J. Park, D. Lee, Y. Kim, J. Kim, J. Lee, J. Park, T. Lee and J. Cho, "Flexible and transparent metallic grid electrodes prepared by evaporative assembly.," *ACS applied materials & interfaces,* vol. 6, no. 15, pp. 12380-12387, 2014.

[37] M. F. Al-Kuhaili, "Characterization of copper oxide thin films deposited by the thermal evaporation of cuprous oxide (Cu2O)," *Vacuum,* vol. 82, no. 6, pp. 623-629, 2008.

[38] J. S. Sharp and J. A. Forrest, "Free surfaces cause reductions in the glass transition temperature of thin polystyrene films," *Physical review letters ,* vol. 91, no. 23, p. 235701, 2003.

[39] P. H. Mayrhofer, C. Mitterer, H. L. and H. Clemens, "Microstructural design of hard coatings," *Materials science,* vol. 51, no. 8, pp. 1032-1114, 2006.

[40] M. Abdelaziz, S. Homaeigohar, M. K. Hedayati, M. A. Assad and M. Elbahri, "Solar Aluminum Kitchen Foils with Omnidirectional Vivid Polarizonic Colors.," *Advanced Optical Materials,* p. 1900737, 2019.

[41] P. B. Johnson and R. W. Christy, "Optical constants of the noble metals," *Physical review B,* vol. 6, no. 12, p. 4370, 1972.

[42] E. Zarie, "Vacuum evaporation of pharmaceutical molecules for the creation of medically active nanostructures with enhanced activities.," PhD diss., Christian-Albrechts Universität Kiel, Kiel, 2013.

[43] E. S. Zarie, V. Kaidas, D. Gedamu, Y. K. Mishra, R. Adelung, F. H. Furkert, R. Scherließ, H. Steckel and B. Groessner-Schreiber, "Solvent free fabrication of micro and nanostructured drug coatings by thermal evaporation for controlled release and increased effects.," *PloS one 7,* vol. 7, no. 8, p. e40746, 2012.

[44] C. A. Neugebauer, L. I. Maissel and R. Glang, Handbook of Thin Film Technology, New York: Mcgraw, 1970.

[45] L. Harris and B. M. Siegel, "A Method for the Evaporation of Alloys," *Journal of Applied Physics,* vol. 19, no. 8, pp. 739-741, 1948.

[46] R. Steudel, "Atomic Structure and Chemical Bonding," in *Chemistry of the Non-Metals*, De Gruyter, 1976, pp. 1-101.

[47] Y. Hirshberg, "Photochromy in the bianthrone series," *Comptes Ren-dus Acad. Sci,* vol. 231, pp. 903-904, 1950.

[48] H. Bouas-Laurent and H. Dur, "Organic Photochromism, IUPAC Technical Report," *Pure Appl. Chem,* vol. 73, no. 4, pp. 639-655, 2001.

[49] S. Kobatake and M. Irie, "8 Photochromism," *Annual Reports Section" C,* vol. 99, pp. 277-313, 2003.

[50] K. Stranius and K. Börjesson, "Determining the photoisomerization quantum yield of photoswitchable molecules in solution and in the solid state," *Scientific reports,* no. 7, p. 41145, 2017.

[51] C. Bohne, M. G. Fan, Z. J. Li, J. Lusztyk and J. C. Scaiano, "Photochromic processes in spiro (1, 3, 3-trimethylindolo-2, 2′-naphth [1, 2-b]-1, 4-oxazine) studied using two-laser two-colour techniques," *Journal of the Chemical Society, Chemical Communications,* vol. 7, pp. 571-572, 1990.

[52] A. Kellmann, F. Tfibel, R. Dubest, P. Levoir, J. Aubard, E. Pottier and R. Guglielmetti, "Photophysics and kinetics of two photochromic indolinospirooxazines and one indolinospironaphthopyran," *Journal of Photochemistry and Photobiology A: Chemistry,* vol. 49, no. 1-2, pp. 63-73, 1989.

[53] D. Eloy and P. Jardon, "Photochromism, thermochromism and solvatochromism of spironaphthoxazines: mechanistic aspects," *Molecular Crystals and Liquid Crystals Science and Technology. Section A. Molecular Crystals and Liquid Crystals,* vol. 246, no. 1, pp. 291-294, 1994.

[54] V. Malatesta, "Photodegradation of organic photochromes," in *Organic Photochromic and Thermochromic Compounds*, Boston, MA, Springer, 2002, pp. 65-166.

[55] R. C. Bertelson, "Reminiscences about organic photochromics," *Molecular Crystals and Liquid Crystals Science and Technology. Section A. Molecular Crystals and Liquid Crystals,* vol. 246, no. 1, pp. 1-8, 1997.

[56] V. Malatesta, G. Ranghino, U. Romano and P. Allegrini, "Photochromic spironaphthoxazines: A theoretical study," *International journal of quantum chemistry*, vol. 42, no. 2, pp. 879-887, 1992.

[57] V. I. Minkin, "hoto-, thermo-, solvato-, and electrochromic spiroheterocyclic compounds.," *Chemical reviews*, vol. 104, no. 5, pp. 2751-2776, 2004.

[58] Q. Chen, Y. Feng, D. Zhang, G. Zhang, Q. Fan, S. Sun and D. Zhu, "Light-Triggered Self-Assembly of a Spiropyran-Functionalized Dendron into Nano-/Micrometer-Sized Particles and Photoresponsive Organogel with Switchable Fluorescence," *Adv. Funct. Mater.*, vol. 20, p. 36–42., 2010.

[59] J. Yan, L. Zhao, C. Li, Z. Hu, G. Zhang, Z. Chen, T. Chen, Z. Huang, J. Zhu and M. Zhu, "Optical nanoimaging for block copolymer self-assembly," *J. Am. Chem. Soc.*, vol. 137, p. 2436–2439, 2015.

[60] M. Irie, "Photochromism: memories and switches introduction," *ACS Publications*, pp. 1683-1684, 2000.

[61] M. Zhu, L. Zhu, J. Han, W. Wu, J. Hurst and A. Li, "Spiropyran-based photochromic polymer," *J. Am. Chem. Soc.*, vol. 128, p. 4303–4309, 2006.

[62] C. Bechinger, S. Ferrere, A. Zaban, J. Sprague and B. Gregg, "Photoelectrochromic windows and displays," *Nature*, vol. 383, no. 6601, p. 608, 1996.

[63] M. Russew and H. M., "Photoswitches: from molecules to materials," *Advanced Materials*, vol. 22, no. 31, p. 22, 3348-3360.

[64] E. U. Kulawardana, Kuruwita-Mudiyanselage and T. Neckers, "Dual responsive poly (N-isopropylacrylamide) hydrogels having spironaphthoxazines as pendant groups," *Journal of Polymer Science Part A: Polymer Chemistry*, vol. 47, no. 13, pp. 3318-3325, 2009.

[65] H. Xia, J. Li, G. Zou, Q. Zhang and C. Jia, "A highly sensitive and reusable cyanide anion sensor based on spiropyran functionalized polydiacetylene vesicular receptors," *Journal of Materials Chemistry A*, vol. 1, no. 36, pp. 10713-10719., 2013.

[66] J. Piard, "Influence of the solvent on the thermal back reaction of one spiropyran," *Journal of Chemical Education,* vol. 91, no. 12, pp. 2105-2111, 2014.

[67] M. Jamali, M. K. Hedayati, B. Mozooni, M. Javaherirahim, R. Abdelaziz, A. U. Zillohu and M. Elbahri, "Photoresponsive transparent conductive metal with a photobleaching nose," *Advanced Materials,* vol. 23, no. 37, pp. 4243-4247, 2011.

[68] L. Bennett and L. Swartzendruber, "Nuclear Magnetic Resonance," in *ASM Metals Handbook Volume 10, Materials Characterization,* ASM International, pp. 572-597.

[69] PerkinElmer, "Differential Scanning Calorimetry (DSC)," PerkinElmer, Inc, Waltham, MA , 2013.

[70] C. Marcott, "Infrared Spectroscopy," in *ASM Metals Handbook Volume 10, Materials Characterization,* 1992, ASM International, pp. 237-271.

[71] D. K. Smith, "Introduction to Diffraction Methods," in *Materials Characterization Vol.10,* ASM Handbook Committee., 1992, pp. 662-869.

[72] K. A. O'Donnell, "Effects of finite stylus width in surface contact profilometry," *Applied optics,* vol. 32, no. 25, pp. 4922-4928, 1993.

[73] V. Holý, J. Kuběna, I. Ohlídal, K. Lischka and W. Plotz, "X-ray reflection from rough layered systems," *Physical Review B,* vol. 47, no. 23, p. 15896, 1993.

[74] C. E. Lyman, J. I. Goldstein, A. D. Roming, P. Echlin, D. C. Joy, D. E. Newbury, D. B.Williams, J. T. Armstrong, C. E. Fiori, E. Lifshin and K. Peters, Scanning Electron Microscopy, X-Ray Microanalysis and Analytical Electron Microscopy, Springer, 1990.

[75] J. I. Goldstein, D. E. Newbury, J. R. Michael, N. W. Ritchie, J. H. J. Scott and D. C. Joy, Scanning electron microscopy and X-ray microanalysis, Springer, 2017.

[76] M. S. Johal, "Characterization at the Nanoscale," in *Understanding Nanomaterials,* CRC Press, 2012, pp. 97-200.

[77] Royal Society of Chemistry , "Ultraviolet - Visible Spectroscopy (UV)," Royal Society of Chemistry , 2009.

[78] Y. Leng, "Light Microscopy," in *Materials Characterization: Introduction to Microscopic and Spectroscopic Methods, Second Edition*, John Wiley & Sons, 2013, pp. 1-45.

[79] A. K. Chibisov and H. Görner, "Photoprocesses in spirooxazines and their merocyanines," *The Journal of Physical Chemistry A,* vol. 103, no. 26, pp. 5211-5216, 1999.

[80] J. Aubard, F. Maurel, G. Buntinx, R. Guglielmetti and G. Levi, "Picosecond time-resolved resonance Raman spectroscopy and vibrational analysis in spirooxazine photochromism," *Molecular Crystals and Liquid Crystals Science and Technology. Section A. Molecular Crystals and Liquid Crystals,* vol. 345, no. 1, pp. 203-208, 2000.

[81] N. Tamai and H. Masuhara, "Femtosecond transient absorption spectroscopy of a spirooxazine photochromic reaction," *Chemical physics letters,* vol. 191, no. 1-2, pp. 189-194, 1992.

[82] H. Xia, K. Xie and G. Zou, "Advances in spiropyrans/spirooxazines and applications based on Fluorescence Resonance Energy Transfer (FRET) with fluorescent materials," *Molecules,* vol. 22, no. 12, p. 2236, 2017.

[83] D. H. Lee, M. Lee, C. Chung, W. H. Lee and I. J. Lee, "Low-temperature NMR and IR spectra of photomerocyanine form of spirophenanthrooxazine," *Chemistry letters,* vol. 32, no. 7, pp. 578-579, 2003.

[84] L. L. Gladkov, Y. D. Khamchukov, I. Y. Sychev and A. V. Lyubimov, " IR spectrum of the closed form of indolinospironaphthooxazine," *Journal of Applied Spectroscopy,* vol. 79, no. 1, pp. 31-37, 2012.

[85] K. Oura, V. G. Lifshits, A. A. Saranin, A. V. Zotov and M. Katayama, Surface science: an introduction, Springer Science & Business Media, 2013.

[86] A. Moldovan, M. Bota, D. Dorobantu, I. Boerasu, D. Bojin, D. Buzatu and M. Enachescu, "Wetting properties of glycerol on silicon, native SiO2, and bulk SiO2 by scanning polarization force microscopy," *Journal of Adhesion Science and Technology,* vol. 28, no. 13, pp. 1277-1287, 2014.

[87] K. Wasa, M. Kitabatake and H. Adachi, "Thin Film Materials and Devices," in *Thin Film Materials Technology - Sputtering of Compound Materials*, William Andrew Publishing/Noyes, 2004, pp. 1-16.

[88] M. Elbahri, "Functional Inorganic materials," Aalto University, Espoo, 2019.

[89] Sycon Instruments, "STM-100/ MF Thickness / Rate Monitor," Sycon Instruments, New York, 1197.

[90] M. Polanyi, "The Potential Theory of Adsorption," *Science ,* vol. 3585, pp. 1010-1013, 1963.

[91] P. Muller, "Glossary of terms used in physical organic chemistry (IUPAC Recommendations 1994)," *Pure and Applied Chemistry*, vol. 66, no. 5, pp. 1077-1184, 1994.

[92] F. Maurel, J. Aubard, P. Millie, J. P. Dognon, M. Rajzmann, R. Guglielmetti and A. Samat, "Quantum Chemical Study of the Photocoloration Reaction in the Napthoxazine Series," *The Journal of Physical Chemistry A,* vol. 110, no. 14, pp. 4759-4771, 2006.

[93] M. Elbahri, A. U. Zillohu, B. Gothe, M. K. Hedayati, R. Abdelaziz, H. J. El-Khozondar, ... and S. Homaeigohar, "Photoswitchable molecular dipole antennas with tailored coherent coupling in glassy composite," *Light: Science & Applications* , vol. 4, no. 7, p. e316, 2015.

[94] M. lbahri, M. Abdelaziz, S. Homaeigohar, A. Elsharawy, M. K. Hedayati, C. Röder, Mamdouh El Haj Assad and R. Abdelaziz, "Plasmonic Metaparticles on a Blackbody Create Vivid Reflective Colors for Naked-Eye Environmental and Clinical Biodetection," *Advanced Materials*, vol. 30, no. 4, p. 1704442, 2018.

[95] L. Raboin, M. Matheron, J. Biteau, T. Gacoin and J. P. Boilot, " Photochromism of spirooxazines in mesoporous organosilica films," *Journal of Materials Chemistry,* vol. 18, no. 27, pp. 3242-3248, 2008.

[96] R. K. Nahar, " Study of the performance degradation of thin film aluminum oxide sensor at high humidity," *Sensors and Actuators B: Chemical,* vol. 63, no. 1-2, pp. 49-54, 2000.

[97] C. Reichardt and T. Welton, "Appendix," in *Solvents and Solvent Effects in Organic Chemistry,* Weinheim, WILEY-VCH Verlag GmbH & Co, 1988, pp. 490-586.

[98] R. E. Honig, "Vapor pressure data for the solid and liquid elements," *RCA Review,* vol. 30, pp. 285-305, 1969.

[99] H. Pulker, Coatings on Glass, Amsterdam: ELSEVIER, 1999.

[100] J. M. González-Leal, "Optical functionalities of dielectric material deposits obtained from a Lambertian evaporation source," *Optical Express,* vol. 15, no. 9, pp. 5451-5459, 2007.

[101] D. Deniz, "Texture evolution in metal nitride (aluminum nitride, titanium nitride, hafnium nitride) thin films prepared by off-normal incidence reactive magnetron sputtering," University of New Hampshire, Durham, 2008.

[103] P. Oelhafen and A. Schüler, "Nanostructured materials for solar energy conversion," *Solar Energy*, vol. 79, no. 2, pp. 110-121, 2005.

[104] J. Rongé, T. Bosserez, D. Martel, C. Nervi, L. Boarino, F. Taulelle, G. D. S. Bordiga and J. A. Martens, "Monolithic cells for solar fuels," *Chemical Society Reviews,* vol. 43, no. 23, pp. 7963-7981, 2014.

[105] M. Elbahri, M. K. Hedayati and M. Abdelaziz, "Active organic dipolar antenna," in *10th International Congress on Advanced Electromagnetic Materials in Microwaves and Optics (METAMATERIALS),* IEEE, 2016.